



NRL/FR/5310--98-9883

Voltage-Controlled Ferroelectric Lens Phased Arrays

J.B.L. RAO
D.P. PATEL
V. KRICHEVSKY

*Radar Analysis Branch
Radar Division*

September 23, 1998

REPORT DOCUMENTATION PAGE			<i>Form Approved OMB No. 0704-0188</i>	
Public reporting burden for this collection of information is estimated to average 1 hour per response, including the time for reviewing instructions, searching existing data sources, gathering and maintaining the data needed, and completing and reviewing the collection of information. Send comments regarding this burden estimate or any other aspect of this collection of information, including suggestions for reducing this burden, to Washington Headquarters Services, Directorate for Information Operations and Reports, 1215 Jefferson Davis Highway, Suite 1204, Arlington, VA 22202-4302, and to the Office of Management and Budget, Paperwork Reduction Project (0704-0188), Washington, DC 20503.				
1. AGENCY USE ONLY (Leave Blank)	2. REPORT DATE September 23, 1998	3. REPORT TYPE AND DATES COVERED Interim		
4. TITLE AND SUBTITLE Voltage-Controlled Ferroelectric Lens Phased Arrays			5. FUNDING NUMBERS PE - 62232N PR - EW32-1-07	
6. AUTHOR(S) J.B.L. Rao, D.P. Patel, and V. Krichevsky				
7. PERFORMING ORGANIZATION NAME(S) AND ADDRESS(ES) Naval Research Laboratory Washington, DC 20375-5320			8. PERFORMING ORGANIZATION REPORT NUMBER NRL/FR/5310--98-9883	
9. SPONSORING/MONITORING AGENCY NAME(S) AND ADDRESS(ES) Office of Naval Research 800 North Quincy Street, ONR 31 Arlington, VA 22217			10. SPONSORING/MONITORING AGENCY REPORT NUMBER	
11. SUPPLEMENTARY NOTES				
12a. DISTRIBUTION/AVAILABILITY STATEMENT Approved for public release; distribution is unlimited.			12b. DISTRIBUTION CODE	
13. ABSTRACT (Maximum 200 words) A new concept for phased arrays is proposed using a voltage-controlled ferroelectric lens. The ferroelectric lens concept uniquely incorporates bulk phase shifting; the array does not contain individual phase shifters but uses ferroelectric material. This will reduce the number of phase shifters from $(n \times m)$ to $(n + m)$, where n is the number of columns and m is the number of rows in a phased array. The number of phase shifter drivers and phase shifter controls is also significantly reduced by using row-column beam steering. Thus, the ferroelectric lens concept can potentially lead to low-cost phased arrays. This report presents the ferroelectric lens concept, theoretical analysis and design, and experimental results. The results indicate that the ferroelectric lens concept is viable and sound. Various phased array configurations using ferroelectric lens are included. A brief discussion on ferroelectric materials is also included.				
14. SUBJECT TERMS Bulk phase shifting Ferroelectric materials/devices Lens antennas			15. NUMBER OF PAGES 50	
			16. PRICE CODE	
17. SECURITY CLASSIFICATION OF REPORT UNCLASSIFIED	18. SECURITY CLASSIFICATION OF THIS PAGE UNCLASSIFIED	19. SECURITY CLASSIFICATION OF ABSTRACT UNCLASSIFIED	20. LIMITATION OF ABSTRACT UL	

CONTENTS

1. INTRODUCTION.....	1
2. DESCRIPTION OF FERROELECTRIC LENS AND ITS OPERATION	1
3. PHASED ARRAY CONFIGURATIONS USING FERROELECTRIC LENS FOR TWO-DIMENSIONAL SCANNING	7
4. FERROELECTRIC MATERIALS	9
5. THEORETICAL ANALYSIS AND EXPERIMENTAL RESULTS.....	9
Analytical Solution.....	10
Optimization and Numerical Results.....	17
Experimental Results.....	21
6. CONCLUSIONS.....	26
ACKNOWLEDGMENTS	28
REFERENCES.....	28
APPENDIX A — Computer Program “HOPT12”	31
APPENDIX B — Computer Program “HINC12”	37
APPENDIX C — Computer Program “HOPT22”	41
APPENDIX D — Computer Program “HINC22”	47

VOLTAGE-CONTROLLED FERROELECTRIC LENS PHASED ARRAYS

1. INTRODUCTION

Phased array antennas can steer transmitted and received signals without mechanically rotating the antenna. Each radiating element of a phased array is normally connected to a phase shifter and a driver, which determines the phase of the signal at each element to form a beam at the desired angle. The most commonly used phase shifters are ferrite and diode phase shifters. Phase shifters using ferroelectric materials have been proposed [1,2]. The cost of a phased array mainly depends on the cost of phase shifters and drivers. A typical array may have several thousand elements and that many phase shifters and drivers; hence, it is very expensive. Therefore, reducing the cost and complexity of the phase shifters, drivers, and controls is an important consideration in the design of phased arrays. The phased array reported here uniquely incorporates bulk phase shifting; the array does not contain individual phase shifters but uses ferroelectric material. This will reduce the number of phase shifters from $(n \times m)$ to $(n + m)$, where n is the number of columns and m is the number of rows in a phased array. The number of phase shifter drivers and phase shifter controls is also significantly reduced by using row-column beam steering. Bulk phase shifting using diodes has been proposed [3] and reasonably developed [4] in the Radant lens. The lens described here uses voltage-controlled ferroelectric, which introduces analog phase shift rather than digital phase shift as in the Radant lens. The ferroelectric lens has the further advantages of smaller lens thickness, higher-power handling capability, and simpler beam steering controls, and it uses less power to control the phase shift compared to the Radant lens. Thus, it leads to low-cost phased arrays. However, it should be noted that the use of row-column steering may limit the level of side lobes that can be achieved. For the present study, it is assumed that ultralow side lobes are not a requirement and, therefore, row-column phase control can be used to significantly reduce the phased array cost.

2. DESCRIPTION OF FERROELECTRIC LENS AND ITS OPERATION

The main feature of the antennas that use ferroelectric material is the change of permittivity with an applied DC control voltage. A lens-type antenna is discussed in this report. Figure 1 shows a dielectric lens made of dielectric slabs sandwiched between conducting plates. Dielectric slabs are made of ferroelectric material whose dielectric constant can be changed by applying and varying the DC electric field (DC voltage sources V_1, V_2, \dots, V_n are used for this purpose, as shown in Fig. 1). If a plane wave is incident on one side of the lens with RF electric field E normal to the conducting plates, the beam coming out on the other side of the lens can be scanned in the E -plane if a linear phase gradient is introduced along the E -plane direction by adjusting the voltages V_1, V_2, \dots, V_n . The corresponding dielectric constants are shown as $\epsilon_1, \epsilon_2, \dots, \epsilon_n$ in Fig. 1.

Figure 1 illustrates the principle of operation of a ferroelectric lens. However, it has some limitations. To reduce the lens complexity and weight, the number of DC control voltages and the number of conducting plates must be minimized. This can be achieved by limiting the space between the

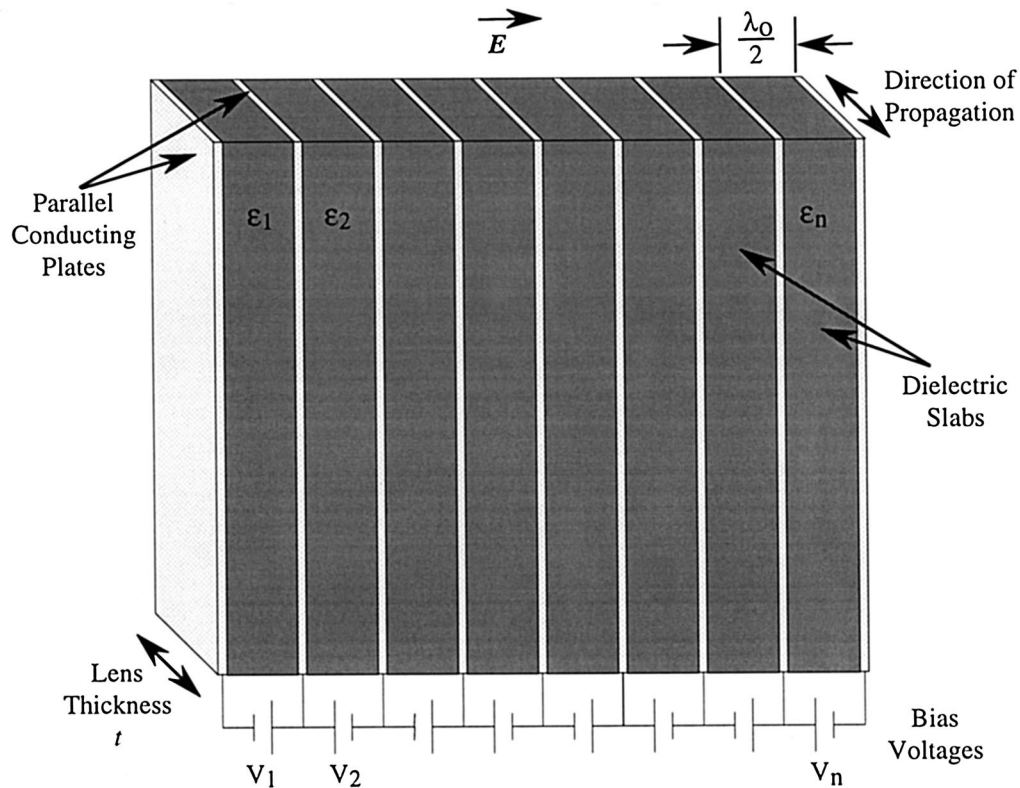


Fig. 1 — Basic configuration of the ferroelectric lens

conducting plates to be less than $\lambda_0/(1 + \sin \phi_s)$, similar to inter-element spacing in any phased array, to avoid grating lobes, where λ_0 is the free-space wavelength, and ϕ_s is the maximum scan angle. Normally, the space between the conducting plates would be $\sim \lambda_0/2$. However, in a ferroelectric lens, this space is filled with a high-dielectric constant ferroelectric material, and the space between the plates is much larger than $\lambda/2$, where λ is the wavelength in the ferroelectric. This means that higher-order modes may propagate. Therefore, to eliminate the problem with higher-order modes, the thickness of the ferroelectric material should be kept to less than $\lambda/2$. In addition, there should be some type of impedance matching arrangement to match the lens surface to free space.

Figure 2 shows a more practical lens configuration. This configuration has several advantages over the basic configuration of Fig. 1. A stepped configuration is used for impedance matching to reduce the amount of dielectric material, to eliminate higher-order mode propagation, and to reduce the bias voltage necessary to create a certain amount of DC electric field intensity within the ferroelectric material. Quarter-wave transformers are used for impedance matching the empty waveguide region to the ferroelectric loaded waveguide region. More than one transformer may be needed, depending on the value of the dielectric constant of the ferroelectric material and the degree of matching needed. Figure 2 also shows a further refinement. This refers to the way the DC bias voltage is applied to the ferroelectric material. An additional center conducting plate is used to bifurcate the ferroelectric material. The DC voltage is applied between this center conducting plate (recessed with respect to parallel plates) and the parallel plates. Since the dielectric material is bifurcated, only half the DC voltage needs to be applied to produce the same DC electric field intensity. It is this DC electric field intensity that controls the dielectric constant of the ferroelectric. In addition, the parallel plates are at ground potential. This makes the handling of the lens safer.

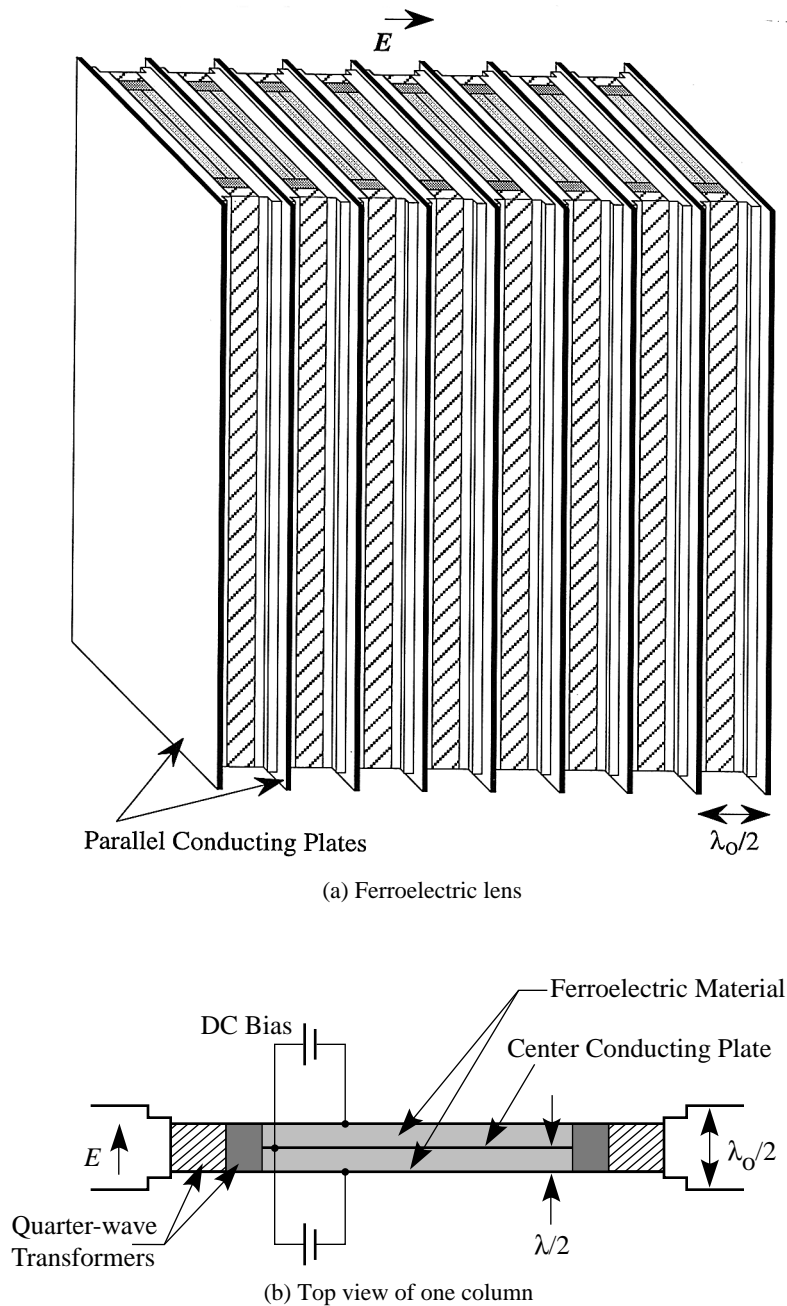


Fig. 2 — A more practical configuration of the ferroelectric lens

The lens thickness needed to use the lens as a scanning antenna can be determined as follows: let t be the lens thickness as shown in Fig. 1, and let the dielectric constant of any one dielectric slab be $\epsilon_{r,\max}$ when no bias voltage is applied. The dielectric constant of a ferroelectric decreases as the bias voltage is increased. Let $\epsilon_{r,\min}$ be the dielectric constant when maximum DC bias is applied. The phase introduced by the slab when no bias voltage is applied is given by

$$\phi_{\max} = \frac{2\pi}{\lambda_0} t \sqrt{\epsilon_{r,\max}}. \quad (1)$$

Similarly, the phase introduced by the same slab, when maximum bias voltage is applied, is given by

$$\phi_{\min} = \frac{2\pi}{\lambda_0} t \sqrt{\epsilon_{r,\min}}. \quad (2)$$

Note the dielectric constant decreases with applied bias voltage. Then the maximum phase change when the maximum bias voltage is applied is

$$\phi_{\max} - \phi_{\min} = \frac{2\pi}{\lambda_0} t \left(\sqrt{\epsilon_{r,\max}} - \sqrt{\epsilon_{r,\min}} \right). \quad (3)$$

For scanning applications, this maximum phase change should be equal to 2π (as in the case of a phase shifter used in a scanning array); hence, Eq. (3) becomes

$$2\pi = \frac{2\pi}{\lambda_0} t \left(\sqrt{\epsilon_{r,\max}} - \sqrt{\epsilon_{r,\min}} \right). \quad (4)$$

So, the thickness of the ferroelectric material needed, in the direction of propagation, to obtain 360° phase shift is

$$t = \frac{\lambda_0}{\sqrt{\epsilon_{r,\max}} - \sqrt{\epsilon_{r,\min}}}. \quad (5)$$

Tunability can be defined for a ferroelectric as the fractional change in the dielectric constant with applied DC bias voltage or

$$\text{Tunability} = \frac{\epsilon_{r,\max} - \epsilon_{r,\min}}{\epsilon_{r,\max}}. \quad (6)$$

Now, Eq. (5) can be written in terms of tunability as

$$\frac{t}{\lambda_0} = \frac{1}{\sqrt{\epsilon_{r,\max}} \left[1 - \sqrt{1 - \text{tunability}} \right]}. \quad (7)$$

So, the thickness of the ferroelectric material needed is a function of the dielectric constant and the tunability of the ferroelectric and the wavelength. The relationship shown in Eq. (7) is illustrated in Fig. 3 for typical ϵ_r of 90 and 120. Additional discussion on this relationship is included later.

Also, it can be shown [5] that the attenuation constant for a uniform plane wave propagating in a low-loss dielectric is

$$\alpha \text{ (dB)} = 27.3 \tan \delta \sqrt{\epsilon_r} \frac{t}{\lambda_0}, \quad (8)$$

where $\tan \delta$ is the loss tangent. Using Eq. (7), we see that to obtain 360° phase shift, the dielectric loss through the ferroelectric is

$$\alpha \text{ (dB)} = \frac{27.3 \tan \delta}{1 - \sqrt{1 - \text{tunability}}}. \quad (9a)$$

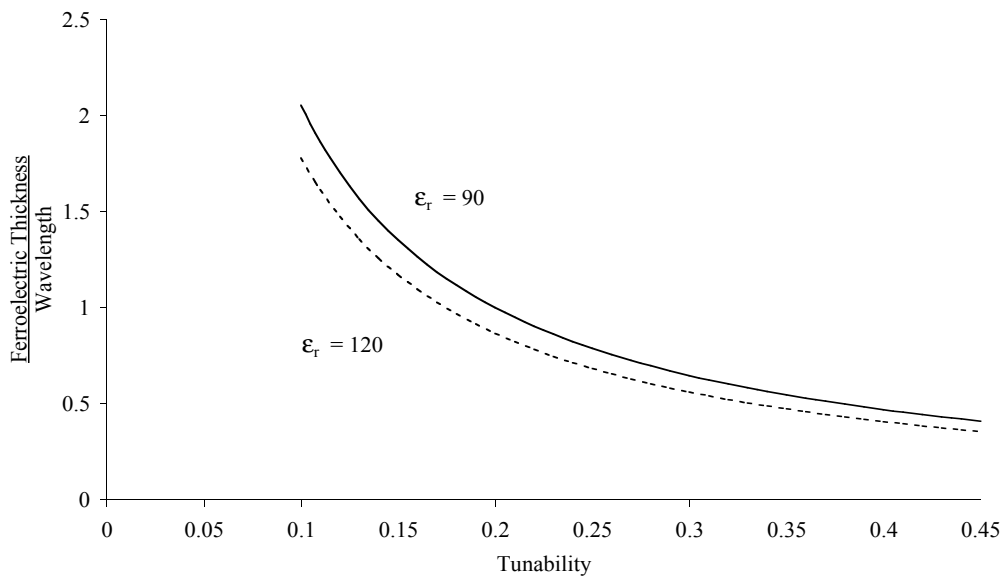


Fig. 3 — Amount of ferroelectric needed for 360° phase shift

It may be noted that the lens loss is independent of the ferroelectric permittivity and depends only on its loss tangent and tunability. Figure 4 plots this equation. It can also be approximated by using the binomial series as

$$\alpha \text{ (dB)} \cong \frac{55 \tan \delta}{\text{tunability}}. \quad (9b)$$

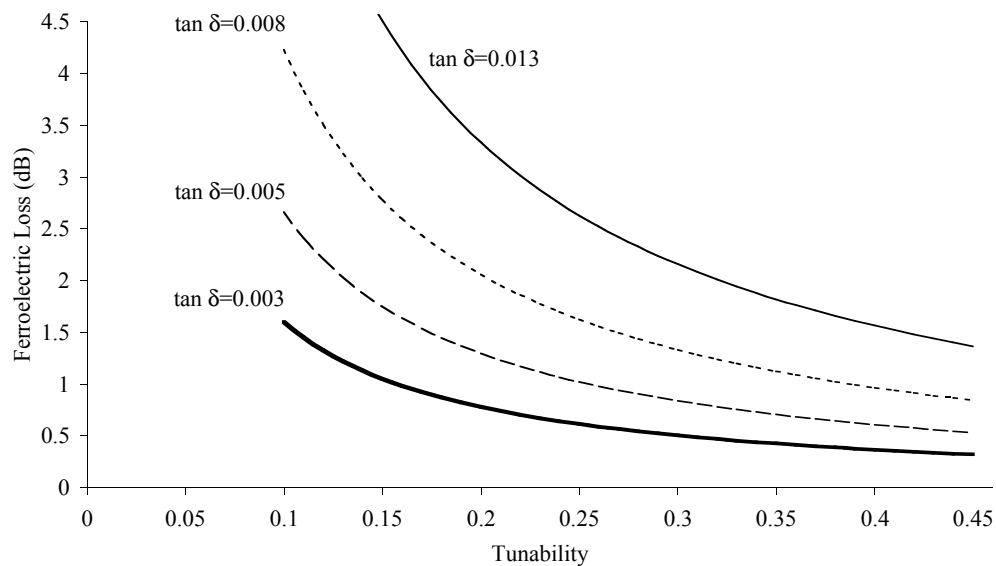


Fig. 4 — Ferroelectric loss for 360° phase shift

In general, the ferroelectrics with higher dielectric constant offer higher tunability, which is desired to reduce the lens thickness. However, matching the lens to free space is easier for smaller ϵ_r . Therefore, a compromise is needed between reducing the lens thickness (to reduce overall lens size) and achieving reasonable impedance match (to reduce reflections from the lens surface). For a typical value of $\epsilon_r \sim 100$, it is possible to obtain a tunability of 20 to 30%, which results in a reasonable lens thickness of $\sim \lambda_0$ (e.g., 3 cm at 10 GHz), as shown in Fig. 3. For this reason, ferroelectric materials with $\epsilon_r \sim 100$ were chosen for the experimental work, which will be discussed later. Figure 4 shows that a $\tan \delta = 0.005$ is needed to limit the lens loss to less than 1 dB. The existing ferroelectric materials are a bit more lossy ($\tan \delta = 0.008$ at 10 GHz) and further research is needed to reduce losses. Additional discussion regarding this will be included when the experimental results are discussed in a later part of the report.

The above theory can be applied to any dielectric whose dielectric constant can be changed by an external stimulus. In addition to ferroelectric materials (which are the focus of this report), liquid crystals are also voltage variable dielectric materials. The dielectric constant of a liquid crystal can be changed by applying a bias voltage, and thus liquid crystals can also be used as phase shifters [6]. Similar to the tunability of a ferroelectric, a liquid crystal has a birefringence defined as

$$\Delta n = \sqrt{\epsilon_{r,\max}} - \sqrt{\epsilon_{r,\min}} . \quad (10a)$$

Unlike the ferroelectric, however, the dielectric constant of the liquid crystal increases with bias voltage. So, $\epsilon_{r,\max}$ is the dielectric constant of the liquid crystal when maximum DC bias is applied, and $\epsilon_{r,\min}$ is the dielectric constant when no bias voltage is applied. Therefore, the thickness of the liquid crystal needed (in the direction of propagation) to obtain 360° phase shift is

$$t = \frac{\lambda_0}{\Delta n} , \quad (10b)$$

and the dielectric loss through the liquid crystal to obtain 360° phase shift is

$$\alpha \text{ (dB)} = \frac{27.3 \tan \delta \sqrt{\epsilon_r}}{\Delta n} . \quad (10c)$$

It is not the purpose of this report to present the application of liquid crystals to phased array antennas. Nevertheless, this report will provide considerable insight into the design of an electronically scanning lens antenna based on liquid crystals because the basic principles and design equations are identical to those of a ferroelectric lens. We will end our discussion of liquid crystals by stating that the main disadvantage of liquid crystals at microwave frequencies is the slow response time of the material when the bias is removed.

The ferroelectric lens offers electronic scanning in one plane. The lens proposed here can be fed by a non-scanning planar array, like a slotted waveguide array. A combination of slotted waveguide array with phase shifters and the lens proposed here can be used as a phased array that can scan in two planes. A space feed can be used with the combination of two lenses proposed here (with a polarization rotator in between) to scan the beam in two planes. The details of these alternatives are discussed in the next section.

3. PHASED ARRAY CONFIGURATIONS USING FERROELECTRIC LENS FOR TWO- DIMENSIONAL SCANNING

A single ferroelectric lens provides one-dimensional (1-D) electronic scanning. Two-dimensional (2-D) scanning can be achieved by cascading two ferroelectric lenses or using one ferroelectric lens in a hybrid configuration with a phased array that can scan in one plane.

Figure 5 shows the cascading of two spatially orthogonal ferroelectric lenses. The first lens provides an elevation scan of a vertically polarized wave. A 90° passive polarization rotator then rotates the electric field to become horizontally polarized. The second lens then provides the azimuth scanning of the horizontally polarized wave. In Fig. 5, a planar array is shown as the illuminator (or feed) for the dual lenses. A space feed can also be used, as shown in Fig. 6, with the dual lens configuration. In this configuration, in addition to scanning the beam, row-column phase controls can also be used to correct the spherical phase errors due to the point space feed; however, this phase correction is not exact, but it is satisfactory for many applications. Spherical phase error corrections for an offset feed configuration is not possible with row-column phase controls. So, offset feeding is not recommended for dual lens configuration.

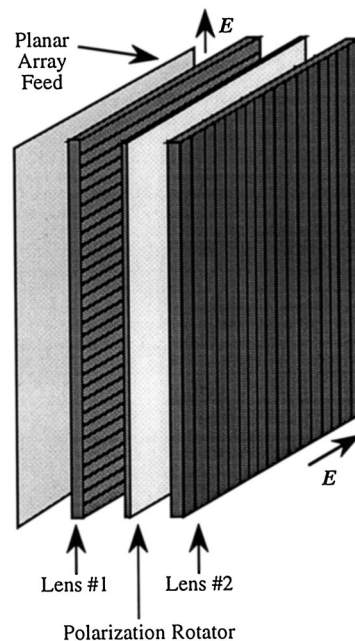


Fig. 5 — Dual lens configuration with a planar array feed

Another method of achieving 2-D scanning uses a hybrid technique in which a conventional planar array with phase shifters provides scanning in one plane and the ferroelectric lens provides the scanning in the other plane. For example, consider a stacked slotted waveguide array with the slots in the narrow wall of the waveguide. Each waveguide is fed through a phase shifter at its input. Scanning in one plane is achieved with these phase shifters. Scanning in the orthogonal plane is obtained by placing a ferroelectric lens in front of the waveguide array, as shown in Fig. 7. For the reasons mentioned before, the cost of the phased arrays that use ferroelectric lens will be much less than the phased arrays that use a phase shifter or a transmit/receive (T/R) module behind each radiating element.

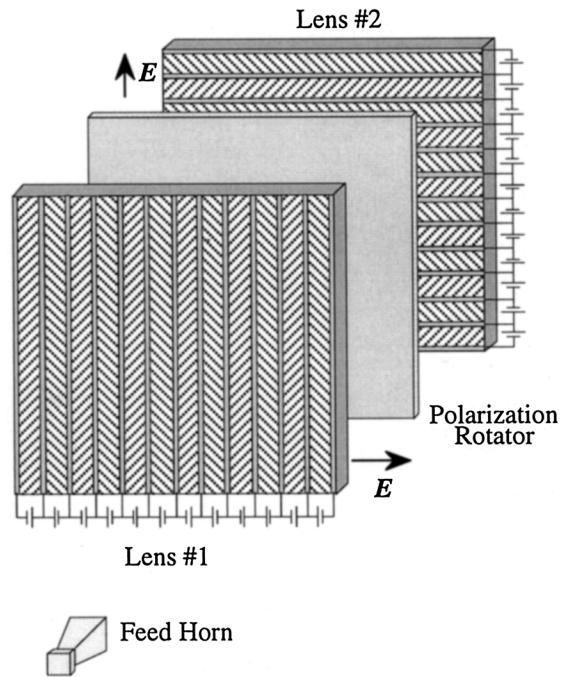


Fig. 6 — Dual lens configuration with a space feed

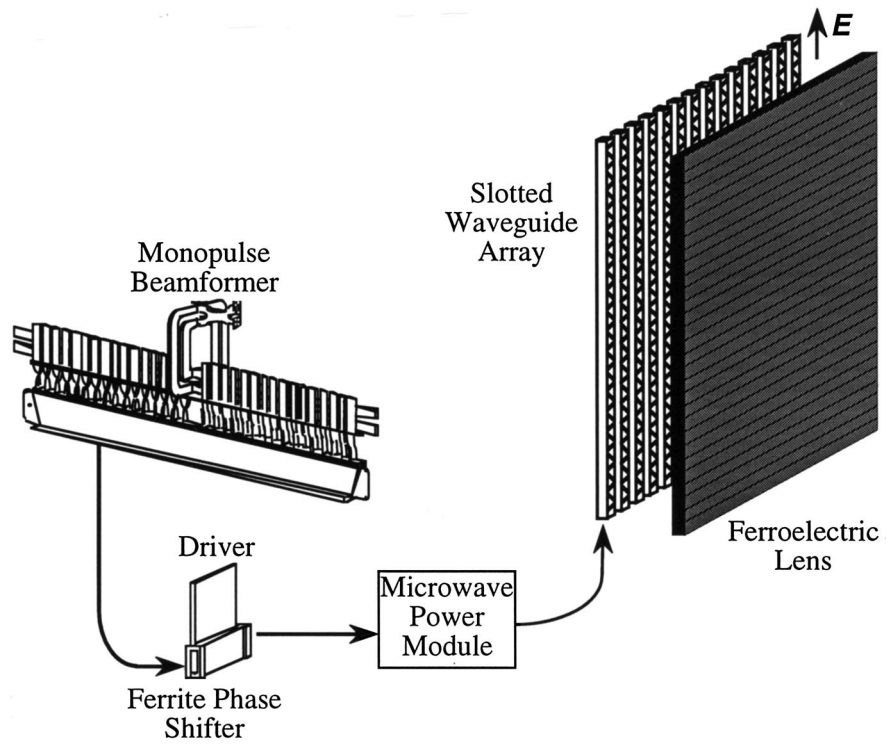


Fig. 7 — Hybrid phased array configuration for 2-D scanning

4. FERROELECTRIC MATERIALS

Ferroelectric materials are nonlinear dielectrics. They possess spontaneous polarization similar to ferromagnetic materials. However, in our application, we use the material in the nonferroelectric (*paraelectric*) state above the Curie temperature, where it is isotropic and provides reciprocal phase shift. The high ϵ_r and $\tan \delta$ of pure ferroelectric materials have limited their applications in phased arrays. Recent improvements in ferroelectric composite materials at the Army Research Laboratory (ARL), Aberdeen Proving Ground, Maryland, prompted renewed interest in developing phase shifters at microwave frequencies. The materials are bulk oxide-ceramic composites of barium strontium titanate oxide (BSTO). ARL has also developed a simple, low-cost processing technique for their manufacturing [7-9]. It involves mixing barium titanate (BaTiO_3) and strontium titanate (SrTiO_3) powders. The resulting BSTO powder is calcined and mixed with an oxide. After pressing and sintering, the composite is ready to be machined. Table 1 lists the properties of several ARL ferroelectric composites at room temperature. The first column indicates the Ba/Sr ratio of the composition. The second column shows the weight percent oxide in the composition. The third column is the Curie temperature. The fourth column is the ferroelectric tunability at 2 V/ μm . The lower the Curie temperature, the more *paraelectric* and less tunable the material becomes at room temperature. The last two columns list ϵ_r and $\tan \delta$ measured at 1 kHz and 10 GHz. Low-frequency results were calculated from capacitance measurements. Measurements at 10 GHz were performed by Dr. R. Geyer at the National Institute of Standards and Technology [10] and confirmed with our measurements. We see that, in general, tunability, ϵ_r , and $\tan \delta$ decrease with decreasing Ba content; they also decrease with increasing oxide content. After oxide is added, ϵ_r changes much less with frequency. As expected for ceramics, $\tan \delta$ increases with frequency; however, it is far lower than that of any other tunable ferroelectrics. Measurements at higher bias voltages indicate that tunability increases linearly with an increase in bias voltage.

Table 1 — Properties of ARL Bulk Ferroelectrics

Material	Oxide (wt %)	Curie Temp.	Tunability (%)	ϵ_r	
				1 kHz / 10 GHz	$\tan \delta \times 10^{-3}$ 1 kHz / 10 GHz
$\text{Ba}_{0.50}\text{Sr}_{0.50}\text{Ti}_3$	0	-25°C	25.5	1908/1099	20.0/18.9
$\text{Ba}_{0.50}\text{Sr}_{0.50}\text{Ti}_3$	20	-55°C	6.44	592/616	0.73/8.7
$\text{Ba}_{0.50}\text{Sr}_{0.50}\text{Ti}_3$	30	-70°C	5.82	414/463	0.7/8.4
$\text{Ba}_{0.50}\text{Sr}_{0.50}\text{Ti}_3$	60	-95°C	3.66	78/84	0.76/6.5
$\text{Ba}_{0.55}\text{Sr}_{0.45}\text{Ti}_3$	30	-45°C	9.54	478/527	0.75/12.1
$\text{Ba}_{0.55}\text{Sr}_{0.45}\text{Ti}_3$	60	-50°C	6.46	95/100	0.34/7.9
$\text{Ba}_{0.60}\text{Sr}_{0.40}\text{Ti}_3$	60	-55°C	9.99	117/118	1.48/12.9

5. THEORETICAL ANALYSIS AND EXPERIMENTAL RESULTS

For the theoretical analysis of the ferroelectric lens, an individual section between two conducting parallel plates of the lens can be considered as one column of a phased array. Initially, the column height is considered infinite in extent and hence it becomes a 2-D parallel plate waveguide with electric field normal to the plates as shown in Fig. 2(b). The lens column fed by a parallel plate waveguide was evaluated assuming transverse electromagnetic (TEM) mode propagation. To eliminate higher-order mode propagation, the ferroelectric slab thickness, between one of the parallel plates and the central conducting plate, is limited to less than $\lambda/2$, as discussed earlier and shown in Fig. 2(b). Theoretical

analysis was also performed using Touchstone, a commonly available software, for a rectangular waveguide with a cross section shown in Fig. 2(b). The analysis was done assuming different column heights (waveguide widths). For widths larger than $4\lambda_0$, the rectangular waveguide results matched well with parallel plate results. For practical reasons, most of the initial measurements were performed in a reduced height X-band rectangular (WR90) waveguide. Theoretical and experimental results for the waveguide configuration, along with a brief description of the ferroelectric lens and its principle of operation, have been reported earlier [11-14]. This report includes the detailed theoretical analysis of the ferroelectric lens, along with the extensive experimental results. Theoretical analysis also indicated that the results are better for a parallel plate waveguide than for a rectangular waveguide.

In this report, for theoretical analysis and numerical results, the geometry was restricted to be 2-D (planar) since each column of the ferroelectric lens is predominantly 2-D, as discussed earlier. Because the lens is to be fed with a linearly polarized field with the electric field normal to the conducting plates, the lens was analyzed only for that case. A single column of the lens, fed by a parallel plate waveguide was evaluated as a parallel plate waveguide. Therefore, the results presented here are for a single column of the lens and do not include the effects of mutual coupling between columns.

Analytical Solution

We have considered two impedance matching networks to match the lens surface to free space over a broad range of frequencies. Both networks use multisection impedance matching transformers. They are shown in Fig. 8, which are the top views of one column. The matching network in Fig. 8(a) uses three transformers. The matching network in Fig. 8(b) uses four transformers. Each transformer is a section of a parallel plate waveguide. In Fig. 8(a):

$$L_i = L_{8-i}, b_i = b_{8-i}, \epsilon_i = \epsilon_{8-i}, \epsilon_4 = \epsilon_r, b_2 = b_3 = b_4 = b,$$

where

$$i = 1, 2, 3.$$

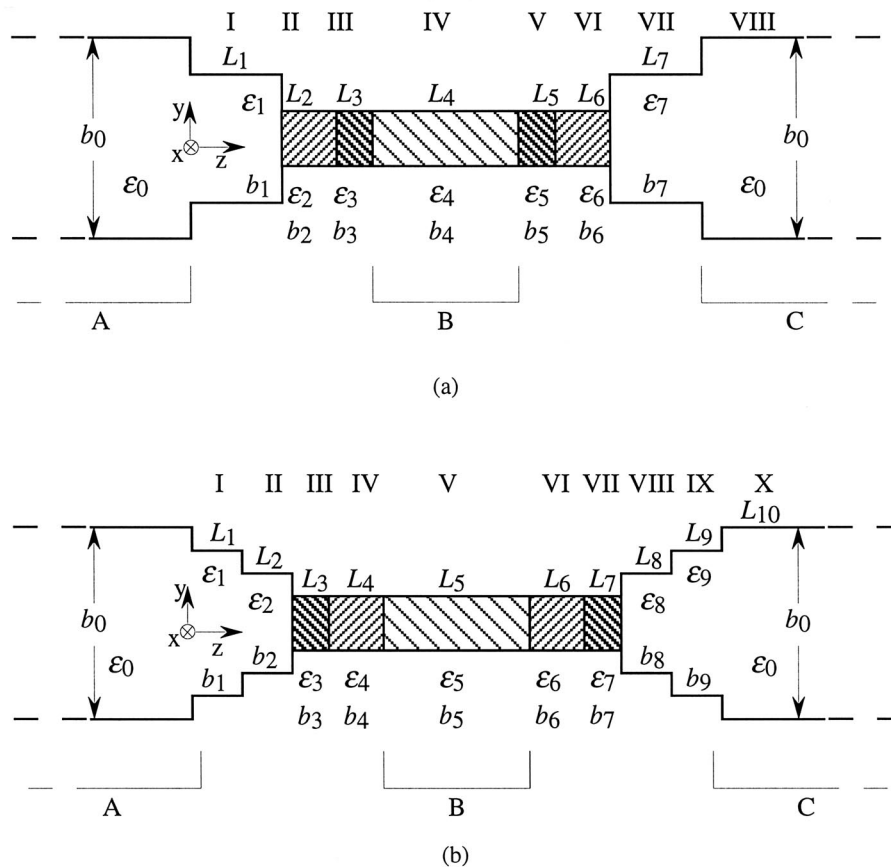
In Figure 8(b):

$$L_i = L_{10-i}, b_i = b_{10-i}, \epsilon_i = \epsilon_{10-i}, \epsilon_5 = \epsilon_r, b_3 = b_4 = b_5 = b,$$

where

$$i = 1, 2, 3, 4.$$

L_i are the lengths of the waveguide sections; b_i are the heights (separations between the parallel plates) of the waveguide sections; ϵ_i are the complex permittivities of the dielectrics completely filling the waveguide sections; and ϵ_r is the dielectric constant of the ferroelectric material. Since the input and output sections of the lens are identical (empty parallel plate waveguide), the same matching network can be used at both ends. The matching network provides impedance matching between the empty semi-infinite parallel plate waveguide (A and C in Fig. 8) and the waveguide section completely filled with the ferroelectric (B in Fig. 8). The heights of waveguides A, B, and C are chosen to assure that only the dominant TEM-mode will propagate in the waveguides and that grating lobes are not formed when an antenna is designed by arraying several columns together. Because waveguide B is filled with a high-dielectric-constant material, its height is chosen to be much smaller than the height of waveguides A and C to eliminate higher-order mode problems. The heights of waveguides A and C are the same and are less than $\lambda_0/2$ at the highest frequency of operation in order to avoid grating lobes.



L_i are lengths of waveguide sections

b_i are the waveguide heights

ϵ_i are the dielectric constants

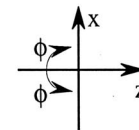


Fig. 8 — Matching networks: (a) three-section matching network, and (b) four-section matching network

The matching network of Fig. 8(a) uses a design with three transformers, where the first transformer is an empty parallel plate waveguide whose height is between that of waveguide A (or C) and B. The other two transformers are parallel plate waveguides completely filled with dielectric materials whose relative permittivities (ϵ_r) are between that of air (or unity) and that of the ferroelectric. Dielectric constant of the first transformer is less than that of the second transformer. The heights of these two transformers are the same as the height of waveguide B. The matching network of Fig. 8(b) uses four transformers, where the first two transformers are empty parallel plate waveguides whose heights are between that of waveguide A (or C) and B. The height of the first transformer is larger than the height of the second transformer. The other two transformers are parallel plate waveguides completely filled with dielectric materials whose relative permittivities are between that of air (or unity) and that of the ferroelectric. The heights of these two transformers are the same as the height of waveguide B. Dielectric constant of the first transformer is less than that of the second transformer.

Since a single ferroelectric lens provides electronic scanning in one plane, another lens or antenna is needed to scan in the second plane. If the first antenna (the one closer to the receiver/transmitter) is a lens, the electromagnetic wave is incident normally on this lens from the feed. This lens will create a phase gradient in one plane, and its radiation will be incident obliquely onto the second lens. For the theoretical

analysis of one column, we assume that the dominant TEM-mode is obliquely incident in the \mathbf{H} -plane. The electric field is orthogonal to the waveguide plates (y -direction). The magnetic field is in the plane parallel to the waveguide walls. The oblique incident angle is measured in the x - z plane. This is the scan angle of the first lens. A time dependency of $\exp(j\omega t)$ is assumed, and the waveguide walls are assumed to be perfect conductors.

As a plane TEM wave is obliquely incident on the matching network from waveguide A, some of the energy associated with the incident wave will be reflected back to waveguide A. We will derive an analytical solution for the reflection coefficient and use this solution to design the optimum matching network, which minimizes the magnitude of the reflected field for a range of incidence angles over the frequency band of interest and for the required change of the ferroelectric dielectric constant to obtain 360° differential phase shift. The case of normal incidence represents a special case of oblique incidence where the incidence angle is zero.

The optimization algorithms were devised and computer programs have been written based on the analytical solutions. As optimization parameters, computer programs use lengths of the transformers, height(s) of the empty waveguide transformer(s), and the dielectric constants of the materials in the last two transformers.

First, consider the matching network which uses four transformers shown in Fig 8(b). Assuming that the dominant TEM-mode is obliquely incident, the electric field in waveguide A can be written as

$$E_y^{(i)} = A_0 \exp[-jk_0(z \cos(\phi) + x \sin(\phi))], \quad (11a)$$

where A_0 is the amplitude of the incident wave; k_0 is the free space wave number, and ϕ is the oblique incidence angle. The magnetic field components of the incident TEM-mode are defined using Maxwell's equations as

$$H_x = \frac{1}{jk_0\mu_0} \frac{\partial E_y}{\partial z} \quad (11b)$$

and

$$H_z = -\frac{1}{jk_0\mu_0} \frac{\partial E_y}{\partial x}, \quad (11c)$$

where μ_0 is the free space permeability. Based on Eqs. (11a) and (11b), the x -component of the incident wave's magnetic field can be expressed as

$$H_x^{(i)} = -A_0 \frac{\cos(\phi)}{\mu_0} \exp[-jk_0(z \cos(\phi) + x \sin(\phi))]. \quad (12)$$

Reflection occurs at the interface between waveguide A and the matching network. The angle of reflection is equal to the angle of incidence. The reflected wave's field components in waveguide A are

$$E_y^{(r)} = R_0 \exp[jk_0(z \cos(\phi) - x \sin(\phi))] \quad (13a)$$

and

$$H_x^{(r)} = R_0 \frac{\cos(\phi)}{\mu_0} \exp[jk_0(z \cos(\phi) - x \sin(\phi))], \quad (13b)$$

where R_0 is the amplitude of the reflected wave.

Since the input and output matching networks are identical, the angle at which the plane wave propagates in waveguide C (area X in Fig. 8(b)) is equal to the angle at which the plane wave was incident in waveguide A. The electric and magnetic fields of the dominant mode in area X can be written as

$$E_y^{(10)} = T_{10} \exp[-jk_0(z \cos(\phi) + x \sin(\phi))] \quad (14a)$$

and

$$H_x^{(10)} = -T_{10} \frac{\cos(\phi)}{\mu_0} \exp[-jk_0(z \cos(\phi) + x \sin(\phi))] , \quad (14b)$$

where T_{10} is the amplitude of the wave in waveguide C (area X).

In area IX of Fig. 8(b), the electromagnetic fields can be represented as a sum of two waves: the first wave travels in the positive z -direction, with an amplitude T_9 ; and the second wave travels in the negative z -direction, with an amplitude R_9 . The fields can be written as

$$E_y^{(9)} = T_9 \exp[-jk_0(z \cos(\phi) + x \sin(\phi))] + R_9 \exp[-jk_0(-z \cos(\phi) + x \sin(\phi))] \quad (15a)$$

and

$$H_x^{(9)} = \frac{\cos(\phi)}{\mu_0} \{-T_9 \exp[-jk_0(z \cos(\phi) + x \sin(\phi))] + R_9 \exp[-jk_0(-z \cos(\phi) + x \sin(\phi))]\} . \quad (15b)$$

T_9 and R_9 are to be determined from the boundary conditions at the interfaces between areas VIII and IX and areas IX and X. The oblique angles of the waves propagating in area IX are the same as in area X because both areas are filled with the same dielectric (air).

The boundary conditions require that the tangential components of electric and magnetic fields be continuous at all discontinuity interfaces. The interface between areas IX and X is at

$$z = d_9 \equiv \sum_{i=1}^9 L_i , \quad (16)$$

and the boundary conditions are

$$E_y^{(10)} = \begin{cases} 0 & \frac{b_9}{2} \leq y \leq \frac{b_0}{2} \\ E_y^{(9)} & -\frac{b_9}{2} \leq y \leq \frac{b_9}{2} \\ 0 & -\frac{b_0}{2} \leq y \leq -\frac{b_9}{2} \end{cases} \quad (17a)$$

and

$$H_x^{(10)} = H_x^{(9)} \quad \frac{-b_9}{2} \leq y \leq \frac{b_9}{2}. \quad (17b)$$

Substituting electric field expressions from Eqs. (14(a)) and (15(a)) into the boundary condition Eq. (17(a)) followed by integration over the interval $[-b_0/2 \leq y \leq b_0/2]$ leads to

$$T_{10}b_0 \exp[-jk_0d_9 \cos(\phi)] = b_9 \{T_9 \exp[-jk_0d_9 \cos(\phi)] + R_9 \exp[jk_0d_9 \cos(\phi)]\}. \quad (18a)$$

Similarly, substituting magnetic field expressions from Eqs. (14(b)) and (15(b)) into the boundary condition Eq. (17(b)) followed by integration over the interval $[-b_9/2 \leq y \leq b_9/2]$ leads to

$$-T_{10} \exp[-jk_0d_9 \cos(\phi)] = -T_9 \exp[-jk_0d_9 \cos(\phi)] + R_9 \exp[jk_0d_9 \cos(\phi)]. \quad (18b)$$

Dividing Eq. (18(a)) by Eq. (18(b)), we get

$$R_9 = T_9 Q_9 \exp[-jk_0 2d_9 \cos(\phi)], \quad (19)$$

where

$$Q_9 = \frac{\left[\frac{b_0}{b_9} - 1 \right]}{\left[\frac{b_0}{b_9} + 1 \right]}. \quad (20)$$

Using Eqs. (19) and (20), the electromagnetic field components $E_y^{(9)}$ and $H_x^{(9)}$ can be expressed as

$$E_y^{(9)} = T_9 \exp[-jk_0(x \sin(\phi) + d_9 \cos(\phi))] \left\{ \exp[-jk_0(z - d_9) \cos(\phi)] + Q_9 \exp[jk_0(z - d_9) \cos(\phi)] \right\} \quad (21a)$$

and

$$H_x^{(9)} = T_9 \frac{\cos(\phi)}{\mu_0} \exp[-jk_0(x \sin(\phi) + d_9 \cos(\phi))] \cdot \left\{ -\exp[-jk_0(z - d_9) \cos(\phi)] + Q_9 \exp[jk_0(z - d_9) \cos(\phi)] \right\}. \quad (21b)$$

In area VIII of Fig. 8(b) the field components can be written as

$$E_y^{(8)} = T_8 \exp[-jk_0(z \cos(\phi) + x \sin(\phi))] + R_8 \exp[-jk_0(-z \cos(\phi) + x \sin(\phi))] \quad (22a)$$

and

$$H_x^{(8)} = \frac{\cos(\phi)}{\mu_0} \left\{ -T_8 \exp[-jk_0(z \cos(\phi) + x \sin(\phi))] + R_8 \exp[-jk_0(-z \cos(\phi) + x \sin(\phi))] \right\}. \quad (22b)$$

The first term corresponds to the wave traveling in the positive z -direction, with an amplitude T_8 , and the second term corresponds to the wave traveling in the negative z -direction, with an amplitude R_8 . T_8 and R_8 are to be determined from the boundary conditions for tangential field components at the interface between areas VIII and IX:

$$z = d_8 \equiv \sum_{i=1}^8 L_i . \quad (23)$$

The boundary conditions are

$$E_y^{(9)} = \begin{cases} 0 & \frac{b_8}{2} \leq y \leq \frac{b_9}{2} \\ E_y^{(8)} & -\frac{b_8}{2} \leq y \leq \frac{b_8}{2} \\ 0 & -\frac{b_9}{2} \leq y \leq -\frac{b_8}{2} \end{cases} \quad (24a)$$

and

$$H_x^{(9)} = H_x^{(8)} \quad \frac{-b_8}{2} \leq y \leq \frac{b_8}{2} . \quad (24b)$$

Substituting electric field expressions from Eqs. (21(a)) and (22(a)) into the boundary conditions of Eq. (24(a)) and integrating over the interval $[-b_9/2 \leq y \leq b_9/2]$, we arrive at

$$\begin{aligned} T_9 \exp(-jk_0 d_9 \cos(\phi)) \cdot \{ \exp(jk_0 L_9 \cos(\phi)) + Q_9 \exp(-jk_0 L_9 \cos(\phi)) \} b_9 \\ = [T_8 \exp(-jk_0 d_8 \cos(\phi)) + R_8 \exp(jk_0 d_8 \cos(\phi))] b_8 . \end{aligned} \quad (25a)$$

Similarly, substituting magnetic field expressions from Eqs. (21(b)) and (22(b)) into the boundary condition Eq. (24(b)) and integrating over the interval $[-b_8/2 \leq y \leq b_8/2]$, we arrive at

$$\begin{aligned} T_9 \exp(-jk_0 d_9 \cos(\phi)) \cdot [-\exp(jk_0 L_9 \cos(\phi)) + Q_9 \exp(-jk_0 L_9 \cos(\phi))] \\ = -T_8 \exp(-jk_0 d_8 \cos(\phi)) + R_8 \exp(jk_0 d_8 \cos(\phi)) . \end{aligned} \quad (25b)$$

Dividing Eq. (25(a)) by (25(b)) we arrive at

$$R_8 = T_8 Q_8 \exp(-jk_0 2d_8 \cos(\phi)) , \quad (26a)$$

where

$$Q_8 = \frac{f_9 + \frac{b_8}{b_9}}{f_9 - \frac{b_8}{b_9}} \quad (26b)$$

$$f_9 = \frac{1 + Q_9 \exp(-jk_0 2L_9 \cos(\phi))}{-1 + Q_9 \exp(-jk_0 2L_9 \cos(\phi))} . \quad (26c)$$

Substitute Eq. (26(a)) into Eqs. (22(a)) and (22(b)), then

$$E_y^{(8)} = T_8 \exp[-jk_0(x \sin(\phi) + d_8 \cos(\phi))] \{ \exp[-jk_0(z - d_8) \cos(\phi)] + Q_8 \exp[jk_0(z - d_8) \cos(\phi)] \} \quad (27a)$$

and

$$H_x^{(8)} = T_8 \frac{\cos(\phi)}{\mu_0} \exp[-jk_0(x \sin(\phi) + d_8 \cos(\phi))] \{ -\exp[-jk_0(z - d_8) \cos(\phi)] + Q_8 \exp[jk_0(z - d_8) \cos(\phi)] \} . \quad (27b)$$

In area VII in Fig. 8(b), the field components can be written as

$$E_y^{(7)} = T_7 \exp[-jk_0(x \sin(\phi) + v_7 z)] + R_7 \exp[-jk_0(x \sin(\phi) - v_7 z)] \quad (28a)$$

and

$$H_x^{(7)} = \frac{v_7}{\mu_0} \{ -T_7 \exp[-jk_0(x \sin(\phi) + v_7 z)] + R_7 \exp[-jk_0(x \sin(\phi) - v_7 z)] \} , \quad (28b)$$

where

$$v_7 = \sqrt{\epsilon_7 - \sin^2(\phi)} . \quad (28c)$$

Continuing this process of writing the transverse electromagnetic field components in each consecutive area and applying boundary conditions at each interface, we arrive at the expression for the dominant mode reflection coefficient in waveguide A:

$$R_0 = \frac{f_1 + \frac{b_0}{b_1}}{f_1 - \frac{b_0}{b_1}} , \quad (29)$$

where

$$Q_i = \frac{\left(\frac{v_i}{v_{i+1}} \right) f_{i+1} + \left(\frac{b_i}{b_{i+1}} \right)}{\left(\frac{v_i}{v_{i+1}} \right) f_{i+1} - \left(\frac{b_i}{b_{i+1}} \right)} , \quad (30)$$

$$f_i = \frac{1 + Q_i \exp[-jk_0 v_i 2L_i]}{-1 + Q_i \exp[-jk_0 v_i 2L_i]} , \quad (31)$$

$$v_i = \sqrt{\epsilon_{ri} - \sin^2(\phi)} , \text{ and} \quad (32)$$

$$i = 1, \dots, M - 1, \quad (33)$$

$$f_M = -1, \text{ and} \quad (34)$$

$$v_M = \cos(\phi), \quad (35)$$

where $M = 10$. To determine the reflection coefficient for the matching network which uses four transformers, f_1 is needed. It is computed iteratively as follows. Initially, $f_{10} = -1$ is used to compute Q_9 , and then f_9 is computed; f_9 is used to compute Q_8 , and so on until f_1 can be computed.

A similar solution was derived for the matching network, which uses three transformers shown in Fig. 8(a). It is expressed by the same set of equations as Eqs. (29)-(35) except now with $M = 8$.

Optimization and Numerical Results

Using the analytical solutions that were developed in the previous section, optimization algorithms based on the minimax approach have been devised that minimize the maximum value of the reflection coefficient. Computer programs (HOPT12, HINC12, HOPT22, and HINC22) have been written to implement these algorithms; a listing of these programs appears in the Appendices. The programs optimize the length of each transformer. For the transformers that use empty parallel plate sections, the height is also optimized. For the last two transformers that use dielectric materials, the programs also optimize their dielectric constants; we use only the dielectric constants of materials that can readily be obtained from manufacturers. The height of the last two transformers is the same as the height of the guide loaded with the ferroelectric material.

The programs provide the optimum values of the matching network parameters that minimize the magnitude of the reflected field for a range of incidence angles over the frequency band of interest and for the required variation of the ferroelectric dielectric constant to obtain 360° differential phase shift. HOPT12 provides the parameters of the optimum transformers for the three-transformer matching network of Fig. 8(a); these parameters are used by HINC12 to compute the reflection coefficient at each frequency, incidence angle, and dielectric constant of interest. HOPT22 and HINC22 perform similar computations for the four-transformer matching network of Fig 8(b).

The computer programs HOPT12 and HINC12 were used to design a matching network with three transformers (Fig. 8(a)). Three scan angle ranges were considered: 0° to 50° , 0° to 55° , and 0° to 60° . For each scan angle range, the optimization was performed over two different frequency bandwidths centered at 10 GHz: 20% (9 to 11 GHz) and 30% (8.5 to 11.5 GHz). It was assumed that $b_0 = 0.4$ in., $b_2 = b_3 = b_4 = 0.1$ in., and $\epsilon_1 = \epsilon_0$. The ferroelectric dielectric constant was assumed to be 100, and its variation was not used for optimization. The minimax optimization minimizes the reflection coefficient over the specified frequency range and scan angles. Table 2 presents the results for each case. For each case, the reflection coefficient will be no greater than the value provided in the table for the specified scan angle and frequency range. If the optimization was performed over a range of ferroelectric dielectric constants, then the reflection coefficients would be slightly larger.

Table 2 — The Maximum Reflection Coefficient
for a Three-Transformer Matching Network

Scan Angle	20% Bandwidth (9 to 11 GHz)	30% Bandwidth (8.5 to 11.5 GHz)
0° to 50°	0.240	0.315
0° to 55°	0.300	0.396
0° to 60°	0.400	0.504

It is evident from Table 2 that the matching network that uses three transformers does not provide a low enough reflection coefficient for a wide range of incidence angles. However, for normal incidence, the reflection coefficient is sufficiently low. The optimization for normal incidence was conducted assuming that the dielectric constant of the ferroelectric varies from 120 to 80 (33% tunability) over a frequency range of 8 to 12 GHz (40% bandwidth), and that $b_0 = 0.4$ in., $b_2 = b_3 = b_4 = 0.1$ in., and $\epsilon_1 = \epsilon_0$. Figure 9 shows the computed results for normal incidence. The corresponding optimum parameters are: $L_1 = 0.2956$ in., $L_2 = 0.1860$ in., $L_3 = 0.0505$ in., $b_1 = 0.2345$ in., $\epsilon_2 = 2.54$, and $\epsilon_3 = 35$. These results were compared with the results obtained by using commercially available software “Touchstone” for a rectangular waveguide. When the width of the rectangular waveguide is chosen to be greater than $4\lambda_0$, the results obtained by Touchstone are identical to results obtained from our computer program for the parallel plate waveguide structure under consideration.

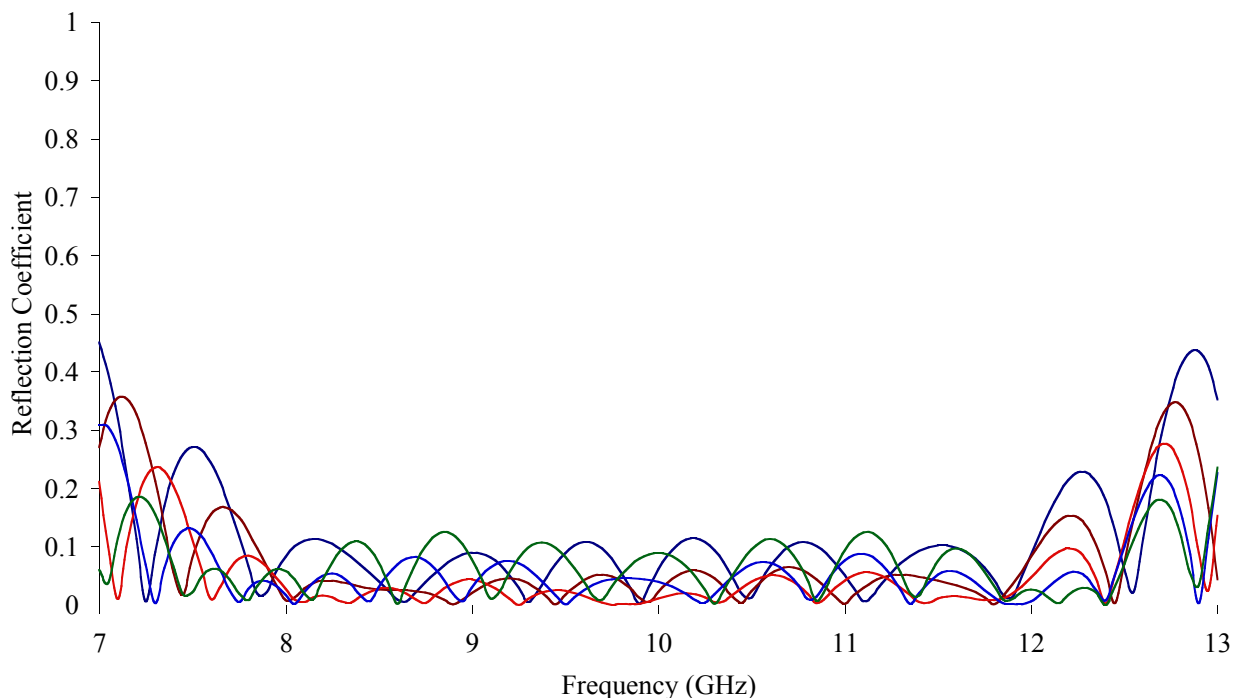


Fig. 9 — Reflection coefficient for normal incidence with three-section matching network for various dielectric constants ($\epsilon_r = 80, 90, 100, 110, \text{ and } 120$)

The matching network that uses four transformers (Fig. 8(b)) provides sufficiently low reflection coefficient even for the case of oblique incidence. The optimization was performed using the computer programs HOPT22 and HINC22 for two operating frequency bands: 9.0 to 11.0 GHz (20% bandwidth) and 8.5 to 11.5 GHz (30% bandwidth). Again, three scan angle ranges were considered: 0° to 50° , 0° to 55° , and 0° to 60° , and it was assumed that: $b_0 = 0.4$ in., $b_3 = b_4 = b_5 = 0.1$ in., and $\epsilon_1 = \epsilon_2 = \epsilon_0$. The unbiased (maximum) dielectric constant of the ferroelectric was assumed to be 100, and three different tunabilities were used in the optimization: 35%, 40%, 45%. Knowing that $\epsilon_{r,\max} = 100$, for each tunability, $\epsilon_{r,\min}$ can be calculated from Eq. (6). $\epsilon_{r,\min}$ is 65, 60, and 55 for tunability of 35%, 40%, and 45%, respectively. To save time, optimization was performed only at the average dielectric constant for each tunability; $\epsilon_{r,\text{avg}}$ is 82.5, 80, and 77.5 for tunability of 35%, 40%, and 45%, respectively. Variation of the dielectric constant was not used in the optimization, although it can be included. The results are provided in Table 3.

Table 3 — The Maximum Reflection Coefficient for a Four-Transformer Matching Network

Scan Angle	20% Bandwidth (9 to 11 GHz)			30% Bandwidth (8.5 to 11.5 GHz)		
	35% Tunability	40% Tunability	45% Tunability	35% Tunability	40% Tunability	45% Tunability
0° to 50°	0.0700	0.0558	0.0538	0.1190	0.1035	0.0960
0° to 55°	0.0922	0.0786	0.0741	0.1432	0.1269	0.1193
0° to 60°	0.1366	0.1144	0.1227	0.1918	0.1769	0.1808

For all three scan angles, the case with 35% tunability provides the largest reflection coefficient. This is because the variation of the dielectric constant was not used in the optimization. Instead, the average ϵ_r was used, and the 35% tunability case has the largest average ϵ_r of 82.5. As it was explained earlier, the larger the ϵ_r , the more difficult the matching problem becomes. It is also not surprising that the 0° to 60° scan angle case provides the largest reflection coefficient for both frequency bandwidths. If the variation of ϵ_r would have been used, the largest reflection coefficient would have been obtained for the case with 30% bandwidth, 0° to 60° scan angle, and 45% tunability. Next, we will use the 35% tunability and 0° to 60° scan angle cases to show that variation of ϵ_r has relatively small effect on the reflection coefficient.

For the case with 35% tunability ($\epsilon_{r,avg} = 82.5$), 0° to 60° scan angle and 20% bandwidth, the optimization is performed for a dielectric constant of 82.5. The optimum parameters are: $L_1 = 0.3736$ in., $L_2 = 0.4186$ in., $L_3 = 0.2116$ in., $L_4 = 0.0539$ in., $b_1 = 0.2913$ in., $b_2 = 0.1627$ in., $\epsilon_3 = 2.54$, and $\epsilon_4 = 30$. Figure 10(a) shows that the reflection coefficient is less than 0.1366, and seven curves are plotted corresponding to seven incidence angles. With all other parameters kept constant, the dielectric constant of the ferroelectric was changed to 65 and 100 to examine the effect of applying DC bias voltage on the reflection coefficient. Figures 10(b) and 10(c) show the results; there is no significant change in the magnitude of the reflection coefficient compared to that of Fig. 10(a).

For the same case, when the optimization is performed for a dielectric constant of 82.5 over 30% bandwidth, the optimum parameters are: $L_1 = 0.3685$ in., $L_2 = 0.4048$ in., $L_3 = 0.2074$ in.; $L_4 = 0.0531$ in., $b_1 = 0.2991$ in., $b_2 = 0.1631$ in., $\epsilon_3 = 2.54$, and $\epsilon_4 = 30$. Figure 11(a) shows that the reflection coefficient is less than 0.1918 for incidence angles up to 60°. As before, with all other parameters kept constant, the dielectric constant of the ferroelectric was changed to 65 and 100 to simulate the effect of applying DC bias voltage. Figures 11(b) and 11(c) show the results. Again, there is no significant change in the magnitude of the reflection coefficient compared to that of Fig 11(a). These results indicated that the lens is well matched even after applying DC bias voltage to scan the beam.

Theoretical results presented in this section indicate that a ferroelectric lens can be designed that is well matched over large scan angles and broad frequency range. The reflection coefficient can be reduced further (or the matching can be improved) by decreasing the frequency bandwidth and/or the range of incidence angles over which the lens operates. If necessary, the matching can also be improved by increasing the number of transformers in the matching network.

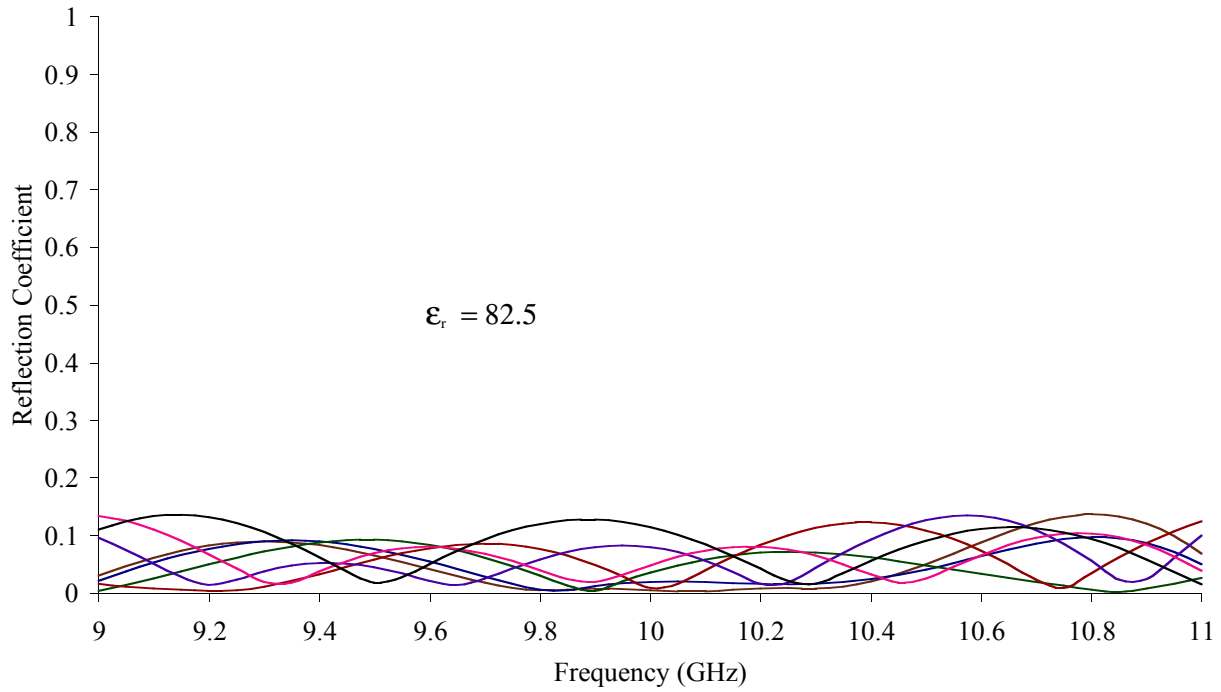


Fig. 10(a) — Reflection coefficient for several incidence angles ($\phi = 0, 10, 20, 30, 40, 50, 60^\circ$), 35% tunability and 20% bandwidth with four-section matching network

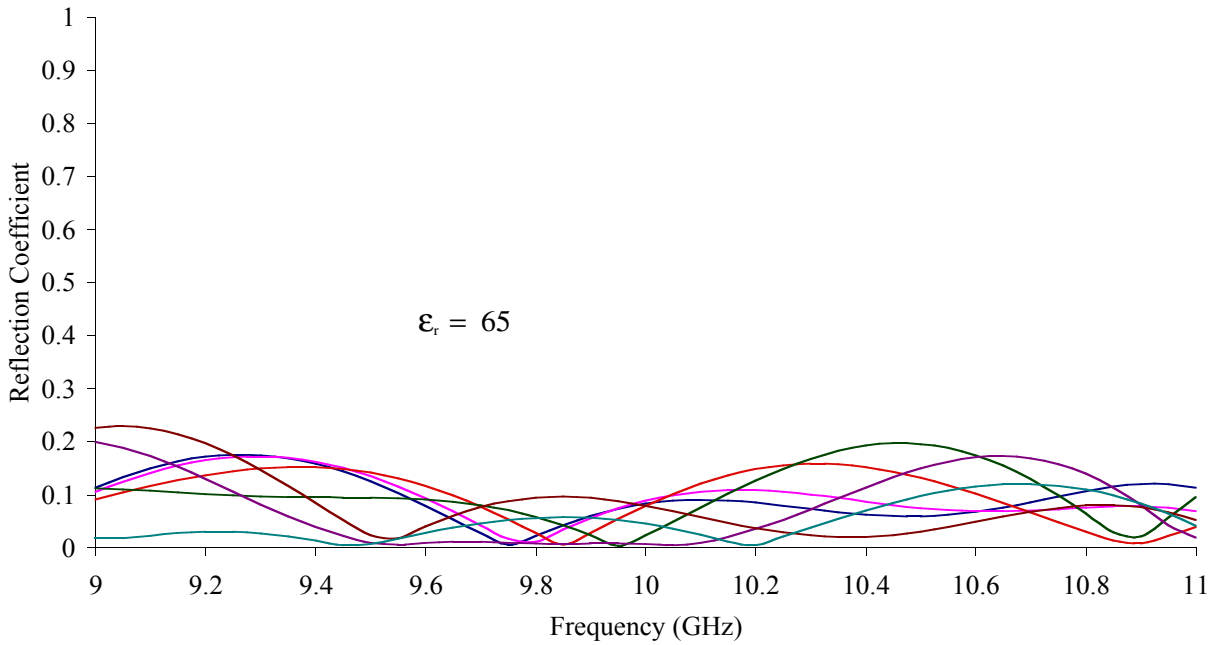


Fig. 10(b) — Reflection coefficient for several incidence angles ($\phi = 0, 10, 20, 30, 40, 50, 60^\circ$), 35% tunability and 20% bandwidth with four-section matching network

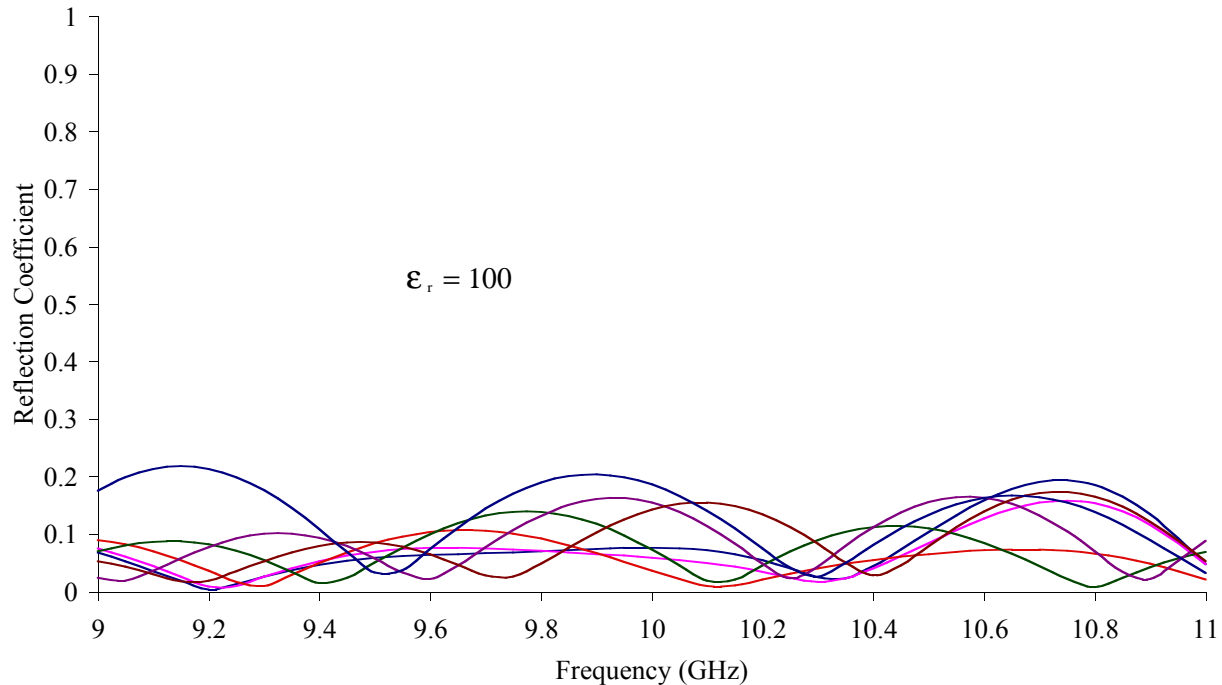


Fig. 10(c) — Reflection coefficient for several incidence angles ($\phi = 0, 10, 20, 30, 40, 50, 60^\circ$), 35% tunability and 20% bandwidth with four-section matching network

EXPERIMENTAL RESULTS

Figure 12 shows the experimental setup. A network analyzer is connected to a WR90 (X-band rectangular) waveguide through a coax-to-waveguide transition. The width of the WR90 is flared from 0.9 in. to 5 in. to create an H -plane horn, which feeds the parallel plate column. The column uses the matching network with three transformers. The transformer parameters were given in the previous section, and Fig. 9 shows the reflection coefficient. The network analyzer measures the s -parameters of the column as a function of frequency and DC bias voltage. The ferroelectrics were 1 in. long (in the direction of propagation), 0.05 in. high, and 5 in. wide. Experiments were performed with two different ferroelectric compositions, $\text{Ba}_{0.60}\text{Sr}_{0.40}\text{TiO}_3$ with 60% oxide (abbreviated 60/60) and $\text{Ba}_{0.55}\text{Sr}_{0.45}\text{TiO}_3$ with 60% oxide (abbreviated 55/60). These two materials offered a good compromise among ϵ_r , $\tan \delta$, and tunability. Table 1 shows properties of these materials; $\epsilon_r = 100$ and $\tan \delta = 0.0079$ for 55/60; and $\epsilon_r = 118$ and $\tan \delta = 0.0129$ for 60/60. Figure 13 shows the measured transmission and reflection coefficients of these two materials. Since the input and output reflection coefficients are almost identical, only one is shown. The reflection coefficient is sufficiently small over a wide frequency band as the theory had predicted in Fig. 9. Because of the higher ϵ_r and the higher $\tan \delta$, 60/60 composition has a higher loss.

Figure 13 also shows that the loss increases with frequency. This is due to two reasons; first, $\tan \delta$ increases with frequency, which is expected for ceramics; second, the electrical length (in terms of wavelengths) of the ferroelectric in the direction of propagation increases with frequency since the physical length is kept constant (1 in.).

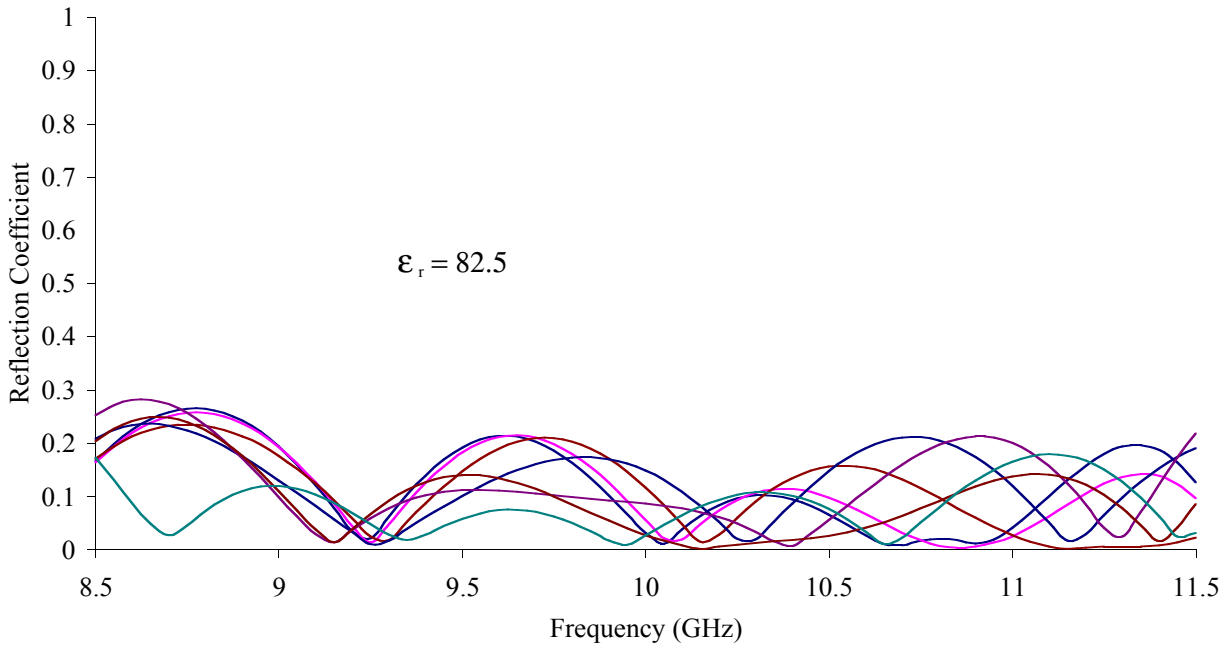


Fig. 11(a) — Reflection coefficient for several incidence angles ($\phi = 0, 10, 20, 30, 40, 50, 60^\circ$), 35% tunability and 30% bandwidth with four-section matching network

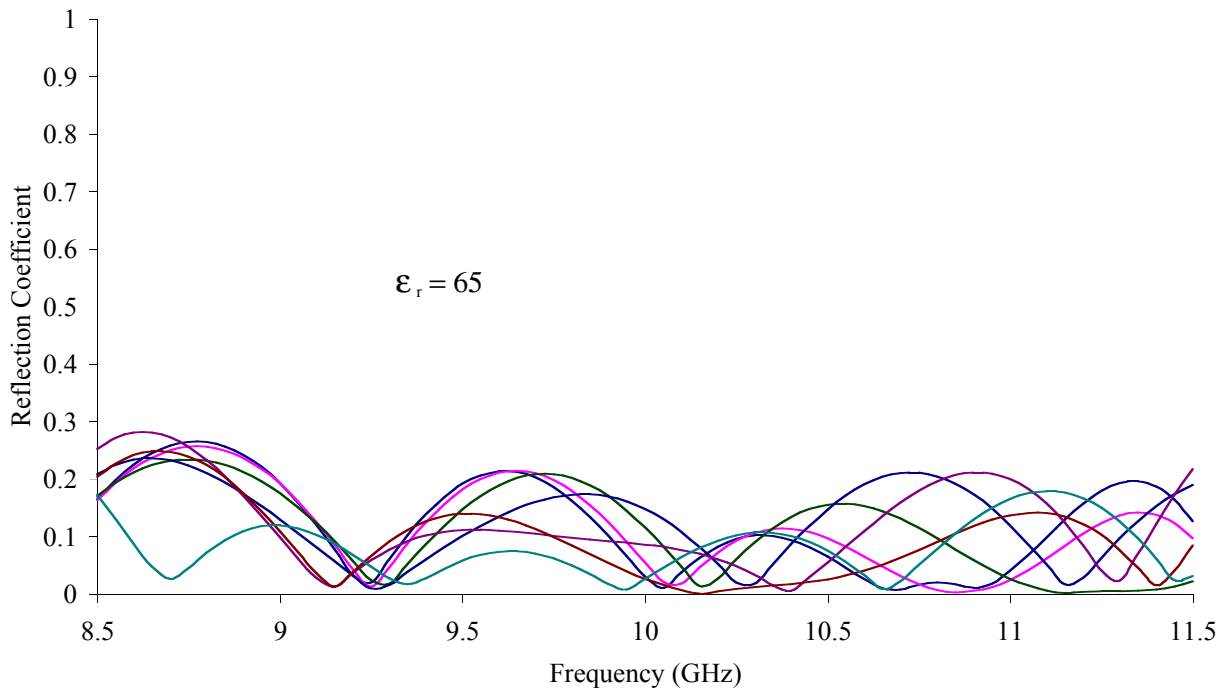


Fig. 11(b) — Reflection coefficient for several incidence angles ($\phi = 0, 10, 20, 30, 40, 50, 60^\circ$), 35% tunability and 30% bandwidth with four-section matching network

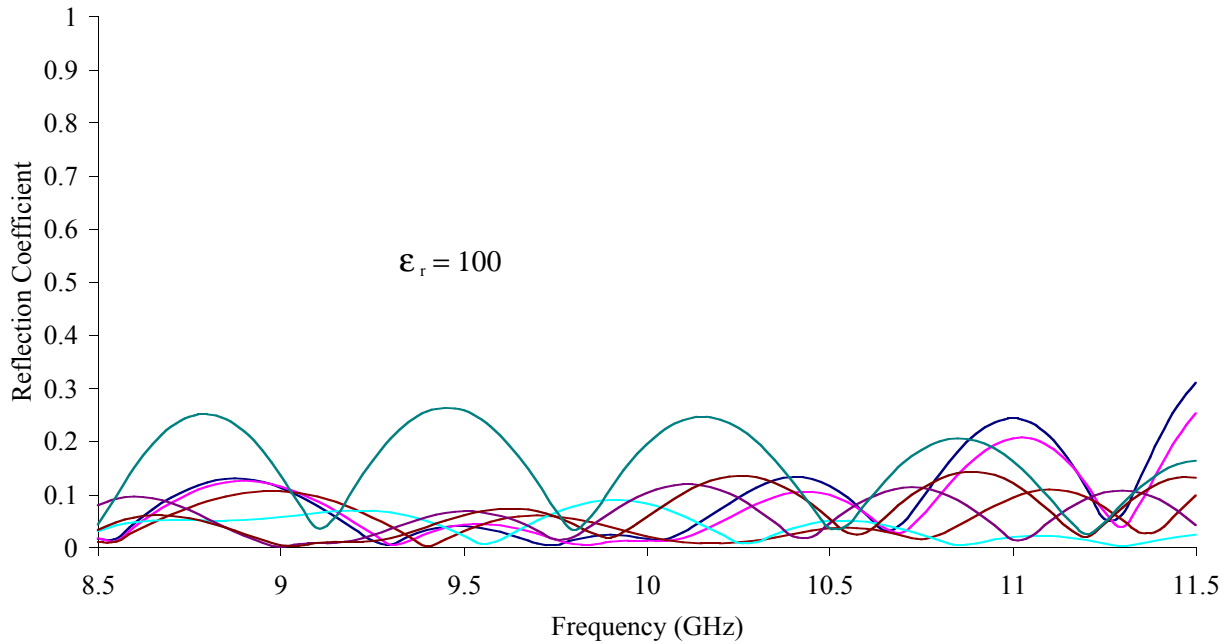


Fig. 11(c) — Reflection coefficient for several incidence angles ($\phi = 0, 10, 20, 30, 40, 50, 60^\circ$), 35% tunability and 30% bandwidth with four-section matching network

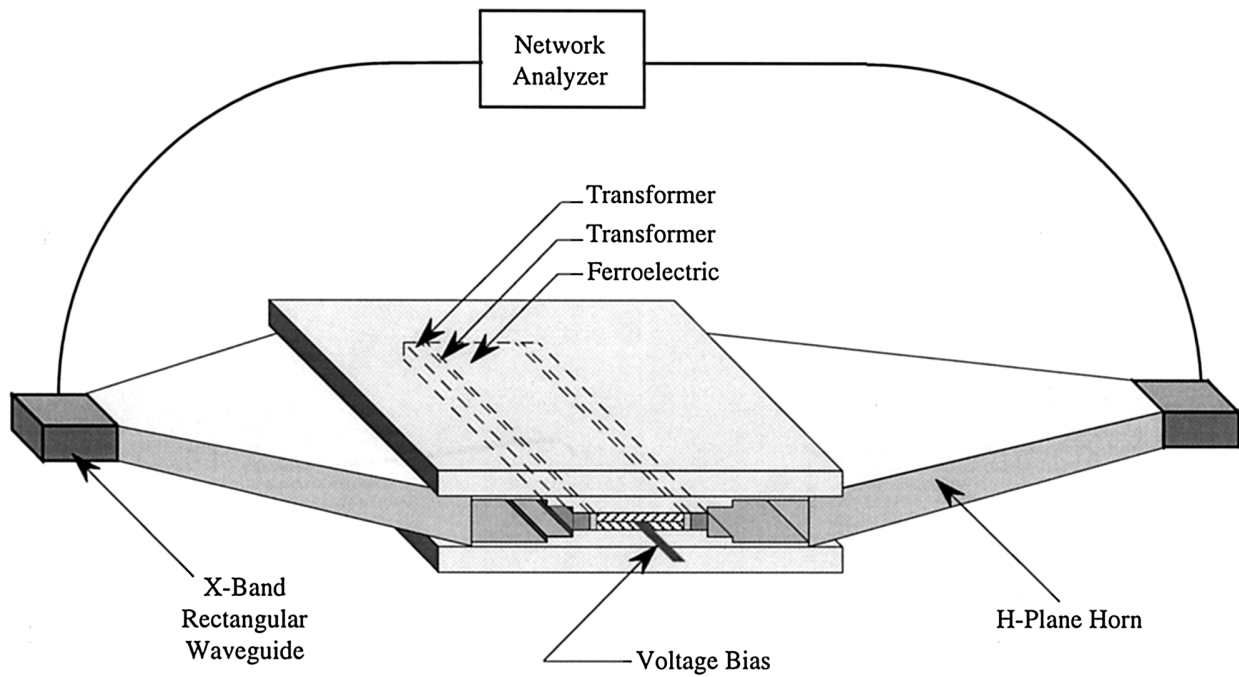


Fig. 12 — Experimental setup for one column

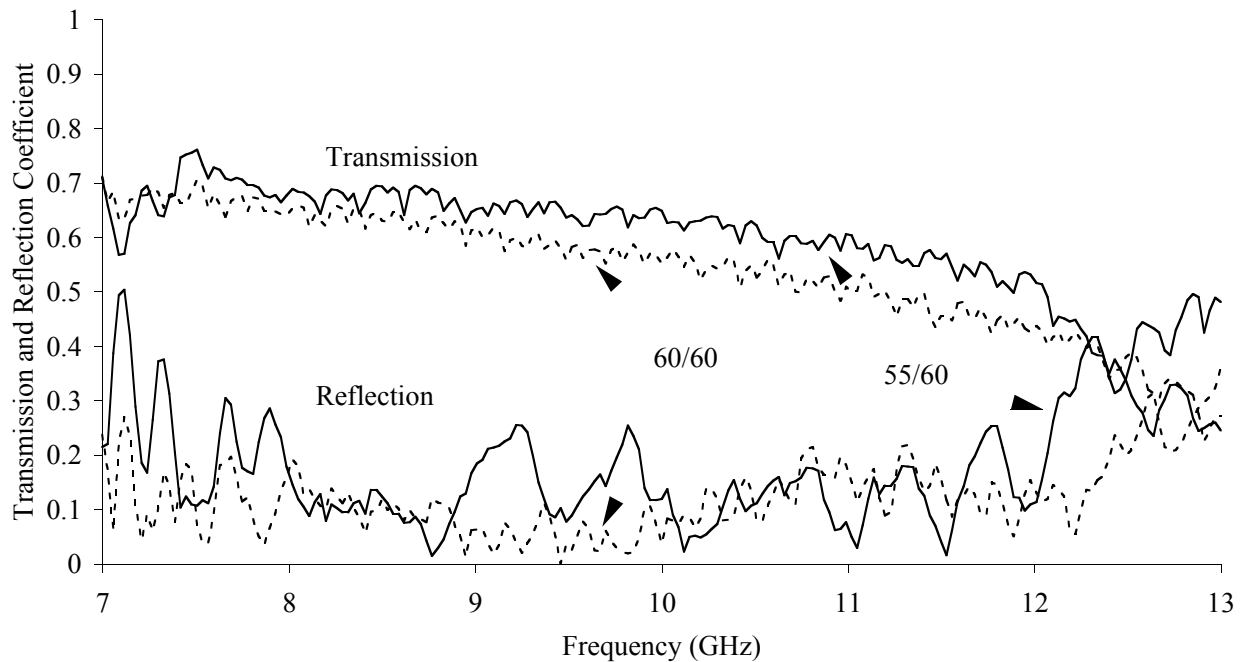


Fig. 13 — Measured voltage transmission and reflection coefficient

As discussed earlier, to minimize the dielectric loss for obtaining 360° differential phase shift, one would like to obtain as high a tunability as possible. Since tunability is a linear function of the DC electric field in the ferroelectric, it is desirable to apply as high a DC electric field as possible. If the dimension across which the DC bias voltage is applied is kept constant, then as the DC bias voltage is increased, the DC electric field increases. Therefore, during experiments, bias voltage was increased gradually until dielectric breakdown occurred. Figures 14(a) and 14(b) show the measured phase shift of the 55/60 and 60/60 ferroelectrics as a function of the bias voltage for various frequencies. Because of the higher barium content, the tunability of the 60/60 material is higher, so the measured phase shift is higher. As expected, the phase shift increases linearly with frequency because the electrical length of the material increases with frequency. Since ferroelectrics are good insulators, the DC current requirements are very low. For example, at 10 kV bias voltage, the DC current drawn was 0.05 mA, so the DC power dissipated is only 0.5 W. The bias voltage can be reduced by further bifurcating the ferroelectrics (using interdigital electrodes) as shown in Fig. 15. Bifurcation reduces the dimension across which the bias voltage is applied; consequently, the required bias voltage is reduced to provide the same DC electric field.

As DC bias voltage is applied to the ferroelectrics, the dielectric constant decreases, which is the basis for obtaining the differential phase shift, but it also complicates the impedance matching problem. However, our design optimization is able to cope with this difficult problem. Figures 16(a) and 16(b) show the reflection coefficients for the 55/60 and 60/60 materials as a function of frequency for various bias voltages. The same parallel plate waveguide, with the same dielectric transformers, is used for both materials. The standing wave ratio (SWR) is less than 2 for frequency range of 8 to 12 GHz, as theoretically predicted earlier.

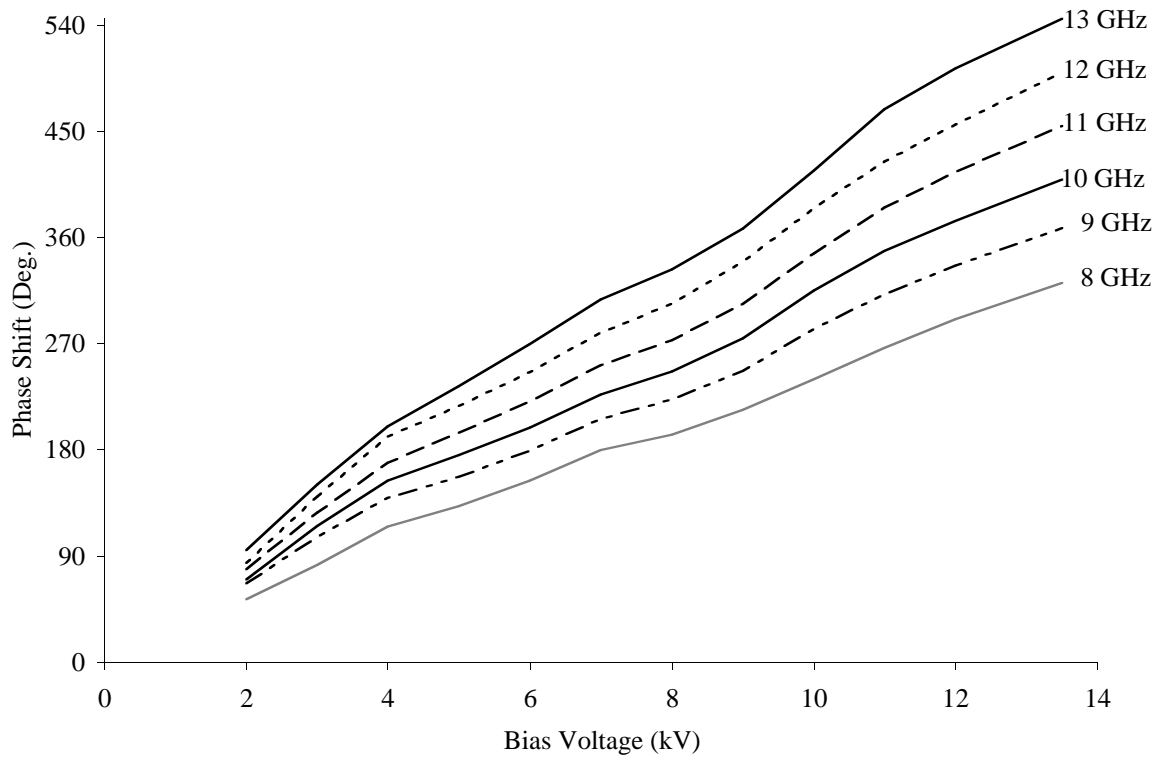


Fig. 14(a) — Measured phase shift with 55/60 ferroelectrics

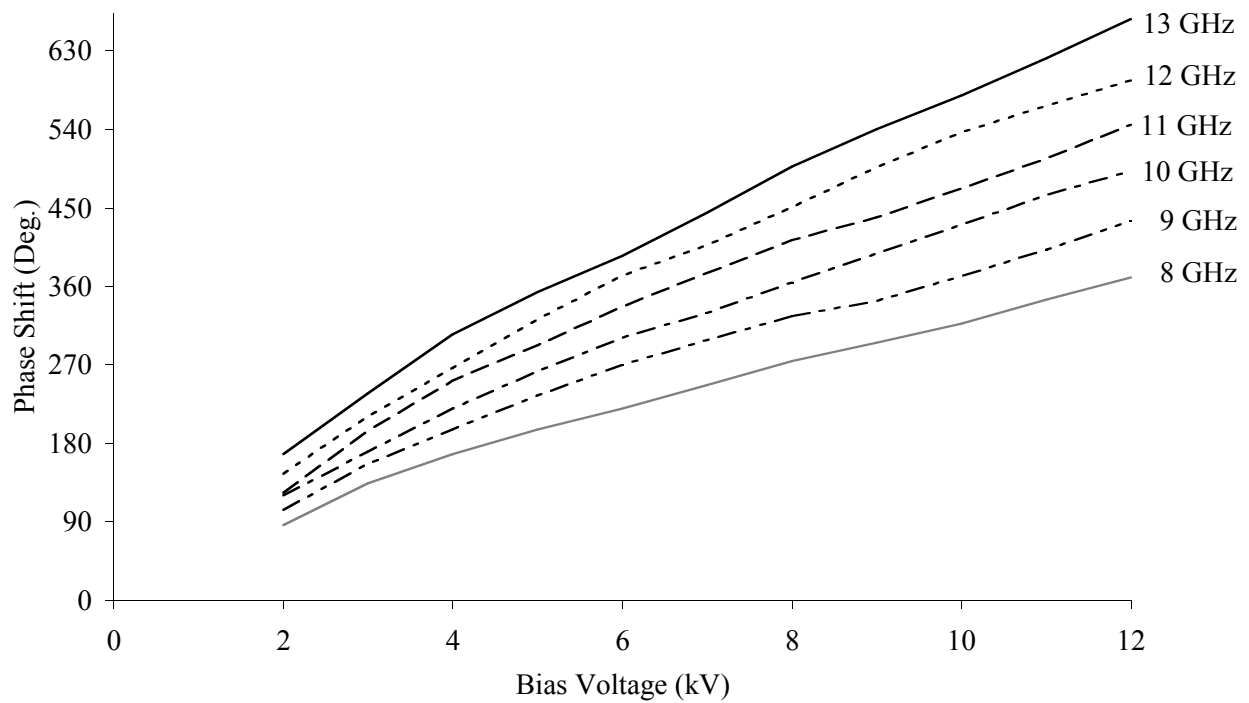


Fig. 14(b) — Measured phase shift with 60/60 ferroelectrics

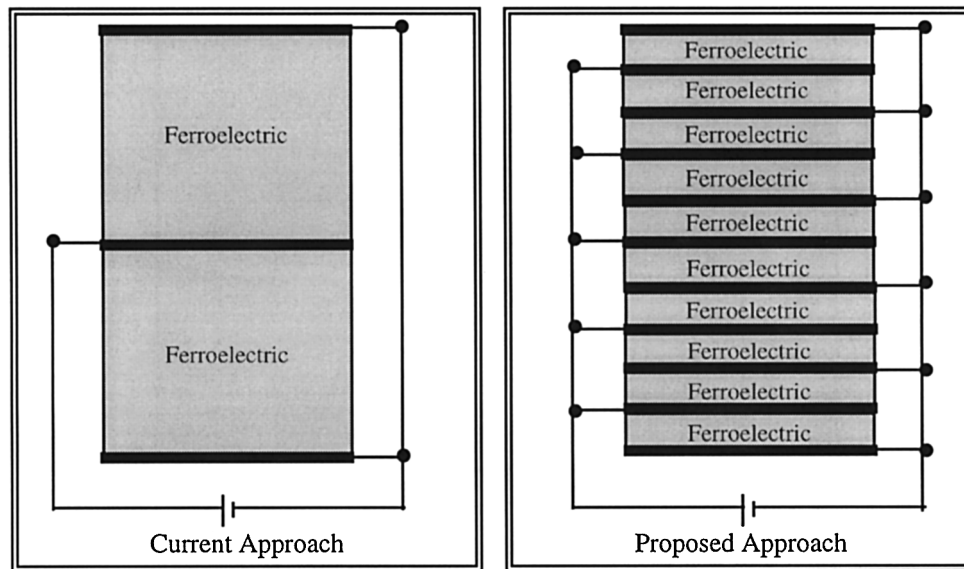


Fig. 15 — Scheme to reduce the bias voltage

Considerable experimentation was performed to gain experience with high-dielectric-constant loaded waveguide. Air gaps between the ferroelectric and the parallel conducting plates cause considerable problems with resonances. Poor electrodes will cause the electric field to concentrate in the air gaps causing breakdown; also, the field in the ferroelectric is reduced, which decreases the ferroelectric tunability. The ferroelectrics are supplied by ARL with the top and bottom surfaces metallized with a baked-on silver ink. When placed in the parallel plate waveguide, the top of the ferroelectric is in contact with the top parallel plate at ground potential, and the bottom of the ferroelectric is in contact with an electrode that is connected to the high-voltage power supply. On the other side of this electrode is the other piece of the ferroelectric whose top is in contact with the high-voltage electrode and whose bottom is in contact with the bottom parallel plate at ground potential. The small air gaps between the ferroelectric and the parallel plates are filled using thin indium sheets and various types of conductive greases and caulks. Indium is used because it has some ductility. It was discovered that air gaps as small as a fraction of a mil can cause problems.

The experimental results presented here agree well with the theoretical results of the lens aperture matching. Control of the column phase shift with the applied DC voltage was also demonstrated experimentally. In summary, the experimental results on one column of the lens proved that the ferroelectric lens concept is viable and sound. Work is continuing in building and demonstrating a small lens.

6. CONCLUSIONS

A new concept for low-cost phased arrays using a voltage controlled ferroelectric lens was proposed. The ferroelectric lens phased array uniquely incorporates bulk phase shifting (the array does not contain discrete phase shifters) using ferroelectric material, which reduces significantly the number of phase shifters and drivers. Furthermore, row-column beam steering is used. These features, in turn, reduce the cost of the phased array. This report presented the ferroelectric lens concept, its theoretical analysis, design, and experimental results. The theoretical results agree well with experimental results, proving that the ferroelectric lens concept is very practical. It was shown that the lens surface can be matched very well to free space over a broad range of frequencies and large scan angles. A number of low-cost phased array configurations using the ferroelectric lens were also described.

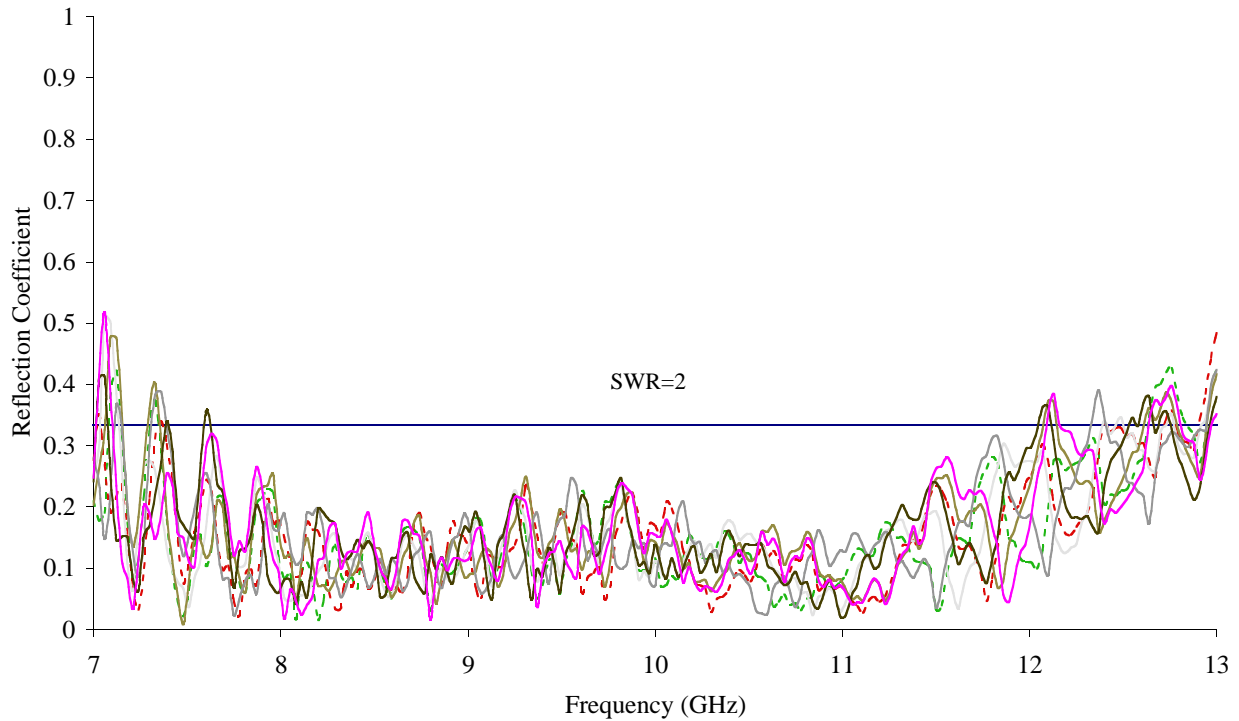


Fig. 16(a) — Measured reflection coefficient with 55/60 ferroelectrics for various bias voltages (0 to 13.5 kV)

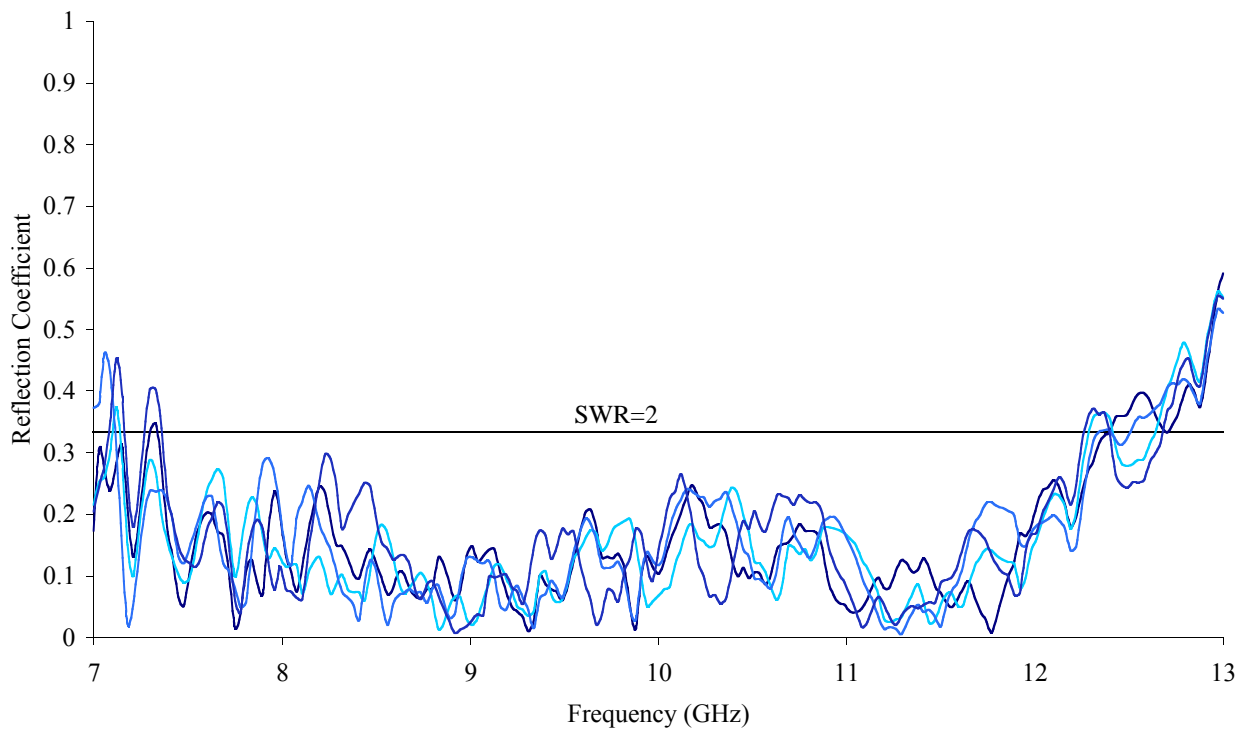


Fig. 16(b) — Measured reflection coefficient with 60/60 ferroelectrics for various bias voltages (0 to 12 kV)

ACKNOWLEDGMENTS

The section on Ferroelectric Materials was contributed mainly by Dr. L. Sengupta of Paratek (formerly with the Army Research Laboratory, Aberdeen Proving Ground, Maryland). The authors thank A. Moffat of SFA, Inc., and J. Valenzi of the Radar Division at the Naval Research Laboratory for their help with the experimental work. This work was supported by the Office of Naval Research, Code ONR 31.

REFERENCES

1. V.K. Varadan, D.K. Ghodgaonkar, V.V. Varadan, J.F. Kelly, and P. Gilkerdas, "Ceramic Phase Shifters for Electronically Steerable Antenna Systems," *Microwave J.* **35**(1), 116-127 (1992).
2. R.W. Babbitt, T.E. Koscica, and W.C. Drach, "Planar Microwave Electro-optic Phase Shifters," *Microwave J.* **35**(6), 63-79 (1992).
3. R.H. Park, "Radant Lens: Alternative to Expensive Phased Arrays," *Microwave J.* **24**(9), 101-105, (1981).
4. J. Leibinger, "Demonstration of Two Axis Electronic Scanning by a Hybrid Radant-TM Lens Array," Final Technical Report No. RL-TR-91-201, Rome Laboratory, Hanscom AFB, Mass., Sept. 1991.
5. S.B. Cohn, "Lens-Type Radiators," in *Antenna Engineering Handbook*, H. Jasik, ed. (McGraw-Hill, New York, 1961), Ch. 14.
6. D. Dolfi, M. Labeyrie, P. Joffre, and J.P. Huignard, "Liquid Crystal Microwave Phase Shifter," *Electron. Lett.* **29**(10), 926-928 (1993).
7. E. Ngo, S. Stowell, L.C. Sengupta, M.E. O'Day, and R. Lancto, "Fabrication and Characterization of Barium Strontium Titanate and Non-Ferroelectric Oxide Composites," in *Mat. Res. Soc. Symp. Proc.* **360**, Boston, Mass., Nov. 28-30, 1994, E.P. George, S. Takahashi, S. Trolrier-McKinstry, K. Uchino, M. Wun-Fogle, eds. (Materials Research Society, Pittsburgh, Pa., 1995), pp. 45-50.
8. L.C. Sengupta, S. Stowell, E. Ngo, M.E. O'Day, and R. Lancto, "Barium Strontium Titanate and Non-Ferroelectric Oxide Ceramic Composites for Use in Phased Array Antennas," *Integr. Ferroelect.* **8**, 77-88 (1995).
9. J.B.L. Rao, D.P. Patel, L.C. Sengupta, J. Synowczynski, L.H. Chiu, E. Ngo, and S. Sengupta, "Ferroelectric Materials for Phased Array Applications," in *Digest of the IEEE Antennas and Propagation Society International Symposium*, Montreal, Canada, July 1997, pp. 2284-2287.
10. R.G. Geyer, J. Krupka, L. Sengupta, and S. Sengupta, "Microwave Properties of Composite Ceramic Phase Shifter Materials," in *Proceedings of the Tenth International Symposium on the Applications of Ferroelectrics (ISAF '96)*, Rutgers University, East Brunswick, N.J., B.M. Kulwicki, A. Amin, and A. Safari, eds. (IEEE, Piscataway, N.J., 1996), pp. 851-854.
11. J.B.L. Rao, "Low Cost Phased Arrays," NRL Memorandum Report 7793, Nov. 1995.

12. J.B.L. Rao and D.P. Patel, "Voltage Controlled Ferroelectric Lens Phased Arrays," in *Digest of the IEEE Antennas and Propagation Society International Symposium*, Baltimore, Md, July 1996, pp. 1624-1627.
13. J.B.L. Rao, G.V. Trunk, and D.P. Patel, "Two Low-Cost Phased Arrays," *Proceedings of the IEEE International Symposium on Phased Array Systems and Technology*, Boston, Mass., Oct. 1996, pp. 119-124.
14. J.B.L. Rao, G.V. Trunk and D.P. Patel, "Two Low-Cost Phased Arrays," *IEEE AES Sys. Mag.* **12**(6), 39-44 (1997).

Appendix A

COMPUTER PROGRAM “HOPT12”

PROGRAM DESCRIPTION

“HOPT12” is an optimization software for the impedance matching network of Fig. 8(a), which uses three transformers. It optimizes the length of all three transformers. The height of the first transformer is also optimized. For the last two transformers, the dielectric constants are also optimized. For the second transformer, the dielectric constants that are used for optimization are 1, 2.54, and 4.3 since these are dielectrics that we can readily obtain. Polystyrene has a dielectric constant of 2.54, and it has always turned out to be the optimum material for the second transformer. For the third transformer, we use the following dielectric constants: 11.6, 13.0, 14.0, 15.0, 16.0, 18.0, 20.0, 30.0, 35.0, 38.0, 40.0, 50.0, 55.0, and 70.0. Again, these values are chosen because we can readily purchase ceramics with these dielectric constants.

The optimization is performed for all combinations of the dielectric constants in the second and third transformers. Input data, which will be requested by the program, are

- a. heights of the waveguides A, B, and C;
- b. length of the waveguide B (length of the ferroelectric); waveguides A and C are assumed to be semi-infinite;
- c. maximum (at zero bias) and minimum (at maximum bias) dielectric constant of the ferroelectric and the step increment to be used for optimization as the dielectric constant is changed from its maximum to minimum value;
- d. maximum scan angle and a step increment;
- e. upper and lower frequency and a step increment; and
- f. value of the dielectric constant of the material in the second transformer.

All lengths are to be entered in inches, frequencies in GHz, and angles in degrees.

The output of the program is written into the file "bbbb.dat". The output consists of data groups for each combination of the second and third transformer dielectric constants. The output parameters are denoted as: b1, the height of the first transformer; and L1, L2 and L3, length of each transformer. For each combination, the program also provides the upper limit for the reflection coefficient, which is denoted in the program's output as "Fvalue" and listed in Table 2 for the cases that we had considered. The matching network with the smallest "Fvalue" is the optimum one.

LISTING OF PROGRAM

```

c      3 transformers optimization
c      -----
common /blk1/ iangle,anglestp,frl,fru,frs,eps2,eps3,allls
common /blk2/ bhl,bhs
common /blk3/ epssin,epssend,epssstep
integer n
parameter (n=4)
integer k,maxfcn,nout,i502,i503,i504,i505,i506
real aaa,hinciden,ftol,fvalue,s,x(n),xguess(n),ai507
real ep3(14),zero
external hincide3,umach,umpol
open (unit=1,file='cccc.dat',status='new')
print *, "Results in file: ccccc.dat"
zero=0.0
ep3(1)=11.6
ep3(2)=13.0
ep3(3)=14.0
ep3(4)=15.0
ep3(5)=16.0
ep3(6)=18.0
ep3(7)=20.0
ep3(8)=30.0
ep3(9)=35.0
ep3(10)=38.0
ep3(11)=40.0
ep3(12)=50.0
ep3(13)=55.0
ep3(14)=70.0
print *, "Enter heights of large and small waveguides (inches)"
read *, bhl,bhs
print *, "Enter length of smaller waveguide (inches)"
read *, allls
print *, "Enter init., final, and step of dielectric constant"
print *, "of smaller waveguide"
read *, epssin,epssend,epssstep
print *, "Enter maximum oblique scan angle and step"
read *, angle,anglestp
iangle=angle/anglestp
print *, "Enter freq. low boundary, upper boundary, freq. step"
read *, frl,fru,frs
print *, "Enter dielectric constant of second transformer"
read *, eps2
do 502 i502=1,14
fv=1000.0
eps3=ep3(i502)
do 503 i503=1,3
xguess(2)=0.1+0.1*(i503-1)
do 504 i504=1,3

```

```

xguess(3)=0.1+0.1*(i504-1)
do 505 i505=1,2
xguess(4)=0.045+0.025*(i505-1)
ai506=0.05
ii506=INT((0.4-0.1)/ai506)-4
do 506 i506=1,ii506
xguess(1)=0.15+ai506*(i506-1)
ftol=1.0e-4
maxfcn=3000
s=1.0
call umpol (hincide3,n,xguess,s,ftol,maxfcn,x,fvalue)
if (fvalue.LT.fv.AND.x(2).GT.zero.AND.x(3).GT.zero.AND.
$x(4).GT.zero.AND.x(4).LE.0.08
$.AND.x(1).GE.0.1.AND.x(1).LE.0.4) then
fv=fvalue
b1=x(1)
al1=x(2)
al2=x(3)
al3=x(4)
end if
506 continue
505 continue
504 continue
503 continue
write(1,778)
778 format(1x,'-----')
write(1,777) eps2,eps3,b1,al1,al2,al3,fv
777 format(1x,' eps2=',f10.4/1x,' eps3=',f10.4/1x,
'$' b1=',f10.4/1x,' L1=',f10.4/1x,' L2=',f10.4/
$1x,' L3=',f10.4/1x,' --- Fvalue---=',f10.4)
502 continue
continue
stop
end
subroutine hincide3 (n,x,f)
implicit real*4 (a-h,o-z)
common /blk1/ iangle,anglestp,frl,fru,frs,eps2,eps3,allls1
common /blk2/ bh11,bhs1
common /blk3/ epssin1,epssend1,epssstp1
integer n
complex qq,ff,fftem1,fftem,qqtem,ref
dimension x(n)
dimension qq(100),ff(100),bh(100),al(100)
dimension eps(100),anu(100),gam(100)
one=1.0
two=2.0
ten=10.0
api=acos(-one)
api2=api/two
apit=api

```

```

api2t=api2
const1=0.16933333
value1=0.0
i234=iangle
aepss=(epssend1-epssin1)/epssstp1
iepss=NINT(aepss)
do 30 i30=1,iepss+1
epss=epssin1+epssstp1*(i30-1)
do 20 i20=1,i234+1
phideg=anglestp*(i20-1)
phi=phideg*api/180.0
bhl=bhl1
bhs=bhs1
allls=allls1
nst=3
nst1=2*nst+1
nst2=2*nst+2
bh(nst+1)=bhs
eps(nst+1)=epss
al(nst+1)=allls
bh(1)=x(1)
bh(2)=bhs
bh(3)=bhs
bh(5)=bh(3)
bh(6)=bh(2)
bh(7)=bh(1)
al(1)=x(2)
al(2)=x(3)
al(3)=x(4)
al(5)=al(3)
al(6)=al(2)
al(7)=al(1)
eps(1)=1.0
eps(2)=eps2
eps(3)=eps3
eps(5)=eps(3)
eps(6)=eps(2)
eps(7)=eps(1)
frequ=fru
freql=frl
frstep=frs
numfr=(frequ-freql)/frstep
do 10 ifr=0,numfr
fr=freql+frstep*ifr
wnum=api*const1*ifr
cccc1=(bhl/bh(7)-one)/(bhl/bh(7)+one)
qq(7)=cmplx(cccc1,0.0)
fftem1=cmplx(0.0,-wnum*two*al(7)*cos(phi))
fftem=exp(fftem1)
ff(7)=(one+qq(7)*fftem)/(-one+qq(7)*fftem)

```

```

anu(6)=sqrt(eps(6)-(sin(phi))**2)
qqtem=(bh(7)/bh(6))*(anu(6)/cos(phi))*ff(7)
qq(6)=(qqtem+one)/(qqtem-one)
fftem1=cmplx(0.0,-wnum*two*al(6)*anu(6))
fftem=exp(fftem1)
ff(6)=(one+qq(6)*fftem)/(-one+qq(6)*fftem)
anu(5)=sqrt(eps(5)-(sin(phi))**2)
qqtem=(anu(5)/anu(6))*ff(6)
qq(5)=(qqtem+one)/(qqtem-one)
fftem1=cmplx(0.0,-wnum*two*al(5)*anu(5))
fftem=exp(fftem1)
ff(5)=(one+qq(5)*fftem)/(-one+qq(5)*fftem)
anu(4)=sqrt(eps(4)-(sin(phi))**2)
qqtem=(anu(4)/anu(5))*ff(5)
qq(4)=(qqtem+one)/(qqtem-one)
fftem1=cmplx(0.0,-wnum*two*al(4)*anu(4))
fftem=exp(fftem1)
ff(4)=(one+qq(4)*fftem)/(-one+qq(4)*fftem)
anu(3)=sqrt(eps(3)-(sin(phi))**2)
qqtem=(anu(3)/anu(4))*ff(4)
qq(3)=(qqtem+one)/(qqtem-one)
fftem1=cmplx(0.0,-wnum*two*al(3)*anu(3))
fftem=exp(fftem1)
ff(3)=(one+qq(3)*fftem)/(-one+qq(3)*fftem)
anu(2)=sqrt(eps(2)-(sin(phi))**2)
qqtem=(anu(2)/anu(3))*ff(3)
qq(2)=(qqtem+one)/(qqtem-one)
fftem1=cmplx(0.0,-wnum*two*al(2)*anu(2))
fftem=exp(fftem1)
ff(2)=(one+qq(2)*fftem)/(-one+qq(2)*fftem)
qqtem=(cos(phi)/anu(2))*ff(2)
qq(1)=(qqtem+bh(1)/bh(2))/(qqtem-bh(1)/bh(2))
fftem1=cmplx(0.0,-wnum*two*al(1)*cos(phi))
fftem=exp(fftem1)
ff(1)=(one+qq(1)*fftem)/(-one+qq(1)*fftem)
ref=(ff(1)+bhl/bh(1))/(ff(1)-bhl/bh(1))
refr=real(ref)
refi=aimag(ref)
refabs=sqrt(refr**2+refi**2)
if (refabs.GT.value1) then
value1=refabs
end if
10 continue
20 continue
30 continu
f=value1
return
end

```

Appendix B

COMPUTER PROGRAM "HINC12"

PROGRAM DESCRIPTION

"HINC12" uses the optimum impedance matching network parameters generated by "HOPT12" for the matching network of Fig. 8(a), which uses three transformers. "HINC12" uses these parameters to compute the reflection coefficient at each frequency, incidence angle, and dielectric constant of interest. The program writes outputs of its calculation into the data file "aaaaa.dat". The output data file consists of four columns: the first column lists the frequency in GHz, the second column gives the absolute value of the reflection coefficient, the third column is the absolute value of the reflection coefficient in dB, and the fourth column is the phase of the reflection coefficient in radians. Input data to the program are

- a. heights of the waveguides A, B, and C;
- b. length of the waveguide B (length of the ferroelectric); waveguides A and C are assumed to be semi-infinite;
- c. dielectric constant of the ferroelectric;
- d. incidence (scan) angle;
- e. upper and lower frequency and a step increment;
- f. dielectric constant of the material in the second and third transformer;
- g. lengths of all three transformers; and
- h. height of the first transformer.

All lengths are to be entered in inches, frequencies in GHz, and angles in degrees.

LISTING OF PROGRAM

```
c   symmetrical transition: 3 transformers
c   -----
implicit double precision (a-h,o-z)
complex qq,ff,fftem1,fftem,qqtem,ref
dimension qq(100),ff(100),bh(100),al(100)
dimension eps(100),anu(100),gam(100)
open (unit=1,file='aaaaa.dat',status='new')
print *, "Results are in file: aaaaa.dat"
one=1.0d0
two=2.0d0
ten=10.0d0
api=acos(-one)
api2=api/two
apit=api
api2t=api2
const1=0.16933333d0
```

```

print *, "Enter incidence angle in degrees"
read (5,*) phideg
phi=phideg*api/180.0d0
print *, "Enter low frequency, upper frequency, freq.step"
read (5,*) freql,frequ,frstep
print *, "Enter larger waveguide height (in inches)"
read (5,*) bhl
print *, "Enter smaller waveguide height (in inches)"
read (5,*) bhs
print *, "Enter smaller waveguide length (in inches)"
read (5,*) allls
print *, "Enter smaller waveguide dielectric constant (relative)"
read (5,*) epss
nst=3
print *, "Enter height of the first transformer (in inches)"
read (5,*) bh(1)
print *, "Enter length of the first transformer (in inches)"
read (5,*) al(1)
print *, "Enter length of the second transformer (in inches)"
read (5,*) al(2)
print *, "Enter length of the third transformer (in inches)"
read (5,*) al(3)
nst1=2*nst+1
nst2=2*nst+2
bh(nst+1)=bhs
eps(nst+1)=epss
al(nst+1)=allls
bh(2)=bhs
bh(3)=bhs
bh(5)=bh(3)
bh(6)=bh(2)
bh(7)=bh(1)
al(5)=al(3)
al(6)=al(2)
al(7)=al(1)
print *, "Enter dielectric constant of the second transformer"
read (5,*) eps(2)
print *, "Enter dielectric constant of the third transformer"
read (5,*) eps(3)
eps(1)=1.0d0
eps(5)=eps(3)
eps(6)=eps(2)
eps(7)=eps(1)
numfr=(frequ-freql)/frstep
do 10 ifr=0,numfr
fr=freql+frstep*ifr
wnum=api*const1*fr
cccc1=(bhl/bh(7)-one)/(bhl/bh(7)+one)
qq(7)=cmplx(cccc1,0.0d0)
fftem1=cmplx(0.0d0,-wnum*two*al(7)*dcos(phi))

```

```

fftem=exp(fftem1)
ff(7)=(one+qq(7)*fftem)/(-one+qq(7)*fftem)
anu(6)=sqrt(eps(6)-(sin(phi))**2)
qqtem=(bh(7)/bh(6))*(anu(6)/cos(phi))*ff(7)
qq(6)=(qqtem+one)/(qqtem-one)
fftem1=cmplx(0.0d0,-wnum*two*al(6)*anu(6))
fftem=exp(fftem1)
ff(6)=(one+qq(6)*fftem)/(-one+qq(6)*fftem)
anu(5)=sqrt(eps(5)-(sin(phi))**2)
qqtem=(anu(5)/anu(6))*ff(6)
qq(5)=(qqtem+one)/(qqtem-one)
fftem1=cmplx(0.0d0,-wnum*two*al(5)*anu(5))
fftem=exp(fftem1)
ff(5)=(one+qq(5)*fftem)/(-one+qq(5)*fftem)
anu(4)=sqrt(eps(4)-(sin(phi))**2)
qqtem=(anu(4)/anu(5))*ff(5)
qq(4)=(qqtem+one)/(qqtem-one)
fftem1=cmplx(0.0d0,-wnum*two*al(4)*anu(4))
fftem=exp(fftem1)
ff(4)=(one+qq(4)*fftem)/(-one+qq(4)*fftem)
anu(3)=sqrt(eps(3)-(sin(phi))**2)
qqtem=(anu(3)/anu(4))*ff(4)
qq(3)=(qqtem+one)/(qqtem-one)
fftem1=cmplx(0.0d0,-wnum*two*al(3)*anu(3))
fftem=exp(fftem1)
ff(3)=(one+qq(3)*fftem)/(-one+qq(3)*fftem)
anu(2)=sqrt(eps(2)-(sin(phi))**2)
qqtem=(anu(2)/anu(3))*ff(3)
qq(2)=(qqtem+one)/(qqtem-one)
fftem1=cmplx(0.0d0,-wnum*two*al(2)*anu(2))
fftem=exp(fftem1)
ff(2)=(one+qq(2)*fftem)/(-one+qq(2)*fftem)
qqtem=(cos(phi)/anu(2))*ff(2)
qq(1)=(qqtem+bh(1)/bh(2))/(qqtem-bh(1)/bh(2))
fftem1=cmplx(0.0d0,-wnum*two*al(1)*cos(phi))
fftem=exp(fftem1)
ff(1)=(one+qq(1)*fftem)/(-one+qq(1)*fftem)
ref=(ff(1)+bhl/bh(1))/(ff(1)-bhl/bh(1))
refr=real(ref)
refi=aimag(ref)
refabs=sqrt(refr**2+refi**2)
refdb=20.0d0*log10(refabs)
refarg=atan(refi/refr)
write (1,20) fr,refabs,refdb,refarg
20 format(1x,f5.2,1x,f8.5,1x,f6.2,
$1x,f8.3)
10 continue
stop
end

```

Appendix C

COMPUTER PROGRAM "HOPT22"

PROGRAM DESCRIPTION

"HOPT22" is an optimization software for the impedance matching network of Fig. 8(b), which uses four transformers. It optimizes the length of all four transformers. The height of the first two transformers is also optimized. For the last two transformers, the dielectric constants are also optimized. For the third transformer, the dielectric constants that are used for optimization are 1, 2.54, and 4.3 since these are dielectrics that we can readily obtain. Polystyrene has a dielectric constant of 2.54, and it has always turned out to be the optimum material for the third transformer. For the fourth transformer, we use the following dielectric constants: 11.6, 13.0, 14.0, 15.0, 16.0, 18.0, 20.0, 30.0, 35.0, 38.0, 40.0, 50.0, 55.0, and 70.0. Again, these values are chosen because we can readily purchase ceramics with these dielectric constants.

The optimization is performed for all combinations of the dielectric constants in the third and fourth transformers. Input data, which will be requested by the program, are

- a. heights of the waveguides A, B, and C;
- b. length of the waveguide B (length of the ferroelectric); waveguides A and C are assumed to be semi-infinite;
- c. maximum (at zero bias) and minimum (at maximum bias) dielectric constant of the ferroelectric, and the step increment to be used for optimization as the dielectric constant is changed from its maximum to minimum value;
- d. maximum scan angle and a step increment;
- e. upper and lower frequency and a step increment; and
- f. value of the dielectric constant of the material in the third transformer.

All lengths are to be entered in inches, frequencies in GHz, and angles in degrees.

The output of the program is written into the file "bbbb.dat". The output consists of data groups for each combination of the third and fourth transformer dielectric constants. The output parameters are denoted as: b1 and b2, the height of the first two transformers, and L1, L2, L3 and L4, length of each transformer. For each combination, the program also provides the upper limit for the reflection coefficient, which is denoted in the program's output as "Fvalue", and listed in Table 3 for the cases that we had considered. The matching network with the smallest "Fvalue" is the optimum one.

LISTING OF PROGRAM

```

c    4 transformers optimization
c    -----
common /blk1/ iangle,anglestp,frl,fru,frs,eps3,eps4,allls
common /blk2/ bhl,bhs
common /blk3/ epssin,epssend,epssstep
integer n
parameter (n=6)
integer k,maxfcn,nout,i507,i502,i503,i504,i505,i506,
$i507,i508
real aaa,hinciden,ftol,fvalue,s,x(n),xguess(n),ai507
real ep4(14),zero
external hincide4,umach,umpol
open (unit=1,file='bbbb.dat',status='new')
print *, "Results in file: bbbbb.dat"
zero=0.0
ep4(1)=11.6
ep4(2)=13.0
ep4(3)=14.0
ep4(4)=15.0
ep4(5)=16.0
ep4(6)=18.0
ep4(7)=20.0
ep4(8)=30.0
ep4(9)=35.0
ep4(10)=38.0
ep4(11)=40.0
ep4(12)=50.0
ep4(13)=55.0
ep4(14)=70.0
print *, "Enter heights of large and small waveguides(inches)"
read *, bhl,bhs
print *, "Enter length of smaller waveguide (inches)"
read *, allls
print *, "Enter init, final, step of dielectric constant"
print *, "of smaller waveguide"
read *, epssin,epssend,epssstep
print *, "Enter maximum oblique scan angle and step"
read *, angle,anglestp
iangle=angle/anglestp
print *, "Enter freq. low boundary, upper boundary, freq. step"
read *, frl,fru,frs
print *, "Enter dielectric constant of third transformer"
read *, eps3
do 502 i502=1,14
fv=1000.0
eps4=ep4(i502)
do 503 i503=1,3
xguess(1)=0.1+0.1*(i503-1)

```

```

do 504 i504=1,2
xguess(2)=0.045+0.025*(i504-1)
do 505 i505=1,3
xguess(3)=0.25+0.05*(i505-1)
do 506 i506=1,2
xguess(4)=0.3+0.1*(i506-1)
ai507=0.05
ii507=INT((xguess(3)-0.1)/ai507)-2
do 507 i507=1,ii507
xguess(5)=0.1+ai507*(i507-1)
do 508 i508=1,2
xguess(6)=0.3+0.1*(i508-1)
ftol=1.0e-4
maxfcn=3000
s=1.0
call umpol (hincide4,n,xguess,s,ftol,maxfcn,x,fvalue)
if (fvalue.LT.fv.AND.x(3).GT.zero.AND.x(3).LT.bhl.AND.
$x(5).GT.zero.AND.
$x(4).GT.zero.AND.x(6).GT.zero.AND.x(1).GT.zero.AND.
$x(2).GT.zero) then
fv=fvalue
b1=x(3)
b2=x(5)
al1=x(4)
al2=x(6)
al3=x(1)
al4=x(2)
end if
508 continue
507 continue
506 continue
505 continue
504 continue
503 continue
write(1,510)
510 format(1x,'-----')
write(1,601) eps3,eps4,b1,b2,al1,al2,al3,al4,fv
601 format(1x,' eps3=',f10.4/1x,' eps4=',f10.4/1x,
&' b1=',f10.4/1x,' b2=',f10.4/1x,
&' L1=',f10.4/1x,' L2=',f10.4/
&1x,' L3=',f10.4/1x,' L4=',f10.4/1x,
&'--- Fvalue --- =',f10.4)
502 continue
write(1,510)
continue
stop
end
subroutine hincide4 (n,x,f)
implicit real*4 (a-h,o-z)
common /blk1/ iangle,anglestp,frl,fru,frs,eps3,eps4,allsl1

```

```

common /blk2/ bh11,bhs1
common /blk3/ epssin1,epssend1,epsssstp1
integer n
complex qq,ff,fftem1,fftem,qqtem,ref
dimension x(n)
dimension qq(100),ff(100),bh(100),al(100)
dimension eps(100),anu(100),gam(100)
one=1.0
two=2.0
ten=10.0
api=acos(-one)
api2=api/two
apit=api
api2t=api2
const1=0.16933333
value1=0.0
aepss=(epssend1-epssin1)/epsssstp1
iepss=NINT(aepss)
do 30 i30=1,iepss+1
epss=epssin1+epsssstp1*(i30-1)
i234=iangle
do 20 i20=1,i234+1
phideg=anglestp*(i20-1)
phi=phideg*api/180.0
bh1=bh11
bhs=bhs1
allls=allls1
nst=4
nst1=2*nst+1
nst2=2*nst+2
bh(nst+1)=bhs
eps(nst+1)=epss
al(nst+1)=allls
bh(1)=x(3)
bh(2)=x(5)
bh(3)=0.1
bh(4)=0.1
bh(6)=bh(4)
bh(7)=bh(3)
bh(8)=bh(2)
bh(9)=bh(1)
al(1)=x(4)
al(2)=x(6)
al(3)=x(1)
al(4)=x(2)
al(6)=al(4)
al(7)=al(3)
al(8)=al(2)
al(9)=al(1)
eps(1)=1.0

```

```

eps(2)=1.0
eps(3)=eps3
eps(4)=eps4
eps(6)=eps(4)
eps(7)=eps(3)
eps(8)=eps(2)
eps(9)=eps(1)
frequ=fru
freql=frl
frstep=frs
numfr=(frequ-freql)/frstep
do 10 ifr=0,numfr
fr=freql+frstep*ifr
wnum=api*const1*fr
cccc1=(bhl/bh(9)-one)/(bhl/bh(9)+one)
qq(9)=cmplx(cccc1,0.0)
fftem1=cmplx(0.0,-wnum*two*al(9)*cos(phi))
fftem=exp(fftem1)
ff(9)=(one+qq(9)*fftem)/(-one+qq(9)*fftem)
anu(8)=sqrt(eps(8)-(sin(phi))**2)
qqtem=(bh(9)/bh(8))*(anu(8)/cos(phi))*ff(9)
qq(8)=(qqtem+one)/(qqtem-one)
fftem1=cmplx(0.0,-wnum*two*al(8)*anu(8))
fftem=exp(fftem1)
ff(8)=(one+qq(8)*fftem)/(-one+qq(8)*fftem)
anu(7)=sqrt(eps(7)-(sin(phi))**2)
qqtem=(bh(8)/bh(7))*(anu(7)/anu(8))*ff(8)
qq(7)=(qqtem+one)/(qqtem-one)
fftem1=cmplx(0.0,-wnum*two*al(7)*anu(7))
fftem=exp(fftem1)
ff(7)=(one+qq(7)*fftem)/(-one+qq(7)*fftem)
anu(6)=sqrt(eps(6)-(sin(phi))**2)
qqtem=(bh(7)/bh(6))*(anu(6)/anu(7))*ff(7)
qq(6)=(qqtem+one)/(qqtem-one)
fftem1=cmplx(0.0,-wnum*two*al(6)*anu(6))
fftem=exp(fftem1)
ff(6)=(one+qq(6)*fftem)/(-one+qq(6)*fftem)
anu(5)=sqrt(eps(5)-(sin(phi))**2)
qqtem=(bh(6)/bh(5))*(anu(5)/anu(6))*ff(6)
qq(5)=(qqtem+one)/(qqtem-one)
fftem1=cmplx(0.0,-wnum*two*al(5)*anu(5))
fftem=exp(fftem1)
ff(5)=(one+qq(5)*fftem)/(-one+qq(5)*fftem)
anu(4)=sqrt(eps(4)-(sin(phi))**2)
qqtem=(bh(5)/bh(4))*(anu(4)/anu(5))*ff(5)
qq(4)=(qqtem+one)/(qqtem-one)
fftem1=cmplx(0.0,-wnum*two*al(4)*anu(4))
fftem=exp(fftem1)
ff(4)=(one+qq(4)*fftem)/(-one+qq(4)*fftem)
anu(3)=sqrt(eps(3)-(sin(phi))**2)

```

```

qqtem=(bh(4)/bh(3))*(anu(3)/anu(4))*ff(4)
qq(3)=(qqtem+one)/(qqtem-one)
fftem1=cplx(0.0,-wnum*two*al(3)*anu(3))
fftem=exp(fftem1)
ff(3)=(one+qq(3)*fftem)/(-one+qq(3)*fftem)
anu(2)=sqrt(eps(2)-(sin(phi))**2)
qqtem=(bh(3)/bh(2))*(anu(2)/anu(3))*ff(3)
qq(2)=(qqtem+one)/(qqtem-one)
fftem1=cplx(0.0,-wnum*two*al(2)*anu(2))
fftem=exp(fftem1)
ff(2)=(one+qq(2)*fftem)/(-one+qq(2)*fftem)
qqtem=(cos(phi)/anu(2))*ff(2)
qq(1)=(qqtem+bh(1)/bh(2))/(qqtem-bh(1)/bh(2))
fftem1=cplx(0.0,-wnum*two*al(1)*cos(phi))
fftem=exp(fftem1)
ff(1)=(one+qq(1)*fftem)/(-one+qq(1)*fftem)
ref=(ff(1)+bhl/bh(1))/(ff(1)-bhl/bh(1))
refr=real(ref)
refi=aimag(ref)
refabs=sqrt(refr**2+refi**2)
if (refabs.GT.value1) then
value1=refabs
end if
10 continue
20 continue
30 continue
f=value1
return
end

```

Appendix D

COMPUTER PROGRAM "HINC22"

PROGRAM DESCRIPTION

"HINC22" uses the optimum impedance matching network parameters generated by "HOPT22" for the matching network of Fig. 8(b), which uses four transformers. "HINC22" uses these parameters to compute the reflection coefficient at each frequency, incidence angle, and dielectric constant of interest. The program writes outputs of its calculation into the data file "aaaaa.dat". The output data file consists of four columns: the first column lists the frequency in GHz, the second column gives the absolute value of the reflection coefficient, the third column is the absolute value of the reflection coefficient in dB, and the fourth column is the phase of the reflection coefficient in radians. Input data to the program are

- a. heights of the waveguides A, B, and C;
- b. length of the waveguide B (length of the ferroelectric); waveguides A and C are assumed to be semi-infinite;
- c. dielectric constant of the ferroelectric;
- d. incidence (scan) angle;
- e. upper and lower frequency and a step increment;
- f. dielectric constant of the material in the third and fourth transformer;
- g. lengths of all four transformers; and
- h. height of the first two transformers.

All lengths are to be entered in inches, frequencies in GHz, and angles in degrees.

LISTING OF PROGRAM

```
c   Symmetrical transition: 4 transformers
c   -----
implicit double precision (a-h,o-z)
complex qq,ff,fftem1,fftem,qqtem,ref
dimension qq(100),ff(100),bh(100),al(100)
dimension eps(100),anu(100),gam(100)
open (unit=1,file='aaaaa.dat',status='new')
print *, "Results are in file:  aaaaa.dat"
one=1.0d0
two=2.0d0
ten=10.0d0
api=acos(-one)
api2=api/two
apit=api
api2t=api2
const1=0.16933333d0
```

```
print *, "Enter incidence angle in degrees"
read (5,*) phideg
phi=phideg*api/180.0d0
print *, "Enter low frequency, upper frequency, freq.step"
read (5,*) freql,frequ,frstep
print *, "Enter larger waveguide height (in inches)"
read (5,*) bhl
print *, "Enter smaller waveguide height (in inches)"
read (5,*) bhs
print *, "Enter smaller waveguide length (in inches)"
read (5,*) allls
print *, "Enter smaller waveguide dielectric constant (relative)"
read (5,*) epss
nst=4
nst1=2*nst+1
nst2=2*nst+2
bh(nst+1)=bhs
eps(nst+1)=epss
al(nst+1)=allls
print *, "Enter height of first transformer (in inches)"
read (5,*) bh(1)
print *, "Enter height of second transformer (in inches)"
read (5,*) bh(2)
bh(3)=bhs
bh(4)=bhs
bh(6)=bh(4)
bh(7)=bh(3)
bh(8)=bh(2)
bh(9)=bh(1)
print *, "Enter length of first transformer (in inches)"
read (5,*) al(1)
print *, "Enter length of second transformer (in inches)"
read (5,*) al(2)
print *, "Enter length of third transformer (in inches)"
read (5,*) al(3)
print *, "Enter length of fourth transformer (in inches)"
read (5,*) al(4)
al(6)=al(4)
al(7)=al(3)
al(8)=al(2)
al(9)=al(1)
print *, "Enter dielectric constant of third transformer"
read (5,*) eps(3)
print *, "Enter dielectric constant of fourth transformer"
read (5,*) eps(4)
eps(1)=1.0d0
eps(2)=1.0d0
eps(6)=eps(4)
eps(7)=eps(3)
eps(8)=eps(2)
```

```

eps(9)=eps(1)
numfr=(frequ-frequl)/frstep
print *, 'numfr=', numfr
do 10 ifr=0, numfr
fr=frequl+frstep*ifr
wnum=api*const1*fr
cccc1=(bhl/bh(9)-one)/(bhl/bh(9)+one)
qq(9)=cplx(cccc1, 0.0d0)
fftem1=cplx(0.0d0, -wnum*two*al(9)*dcos(phi))
fftem=exp(fftem1)
ff(9)=(one+qq(9)*fftem)/(-one+qq(9)*fftem)
anu(8)=sqrt(eps(8)-(sin(phi))**2)
qqtem=(bh(9)/bh(8))*(anu(8)/cos(phi))*ff(9)
qq(8)=(qqtem+one)/(qqtem-one)
fftem1=cplx(0.0d0, -wnum*two*al(8)*anu(8))
fftem=exp(fftem1)
ff(8)=(one+qq(8)*fftem)/(-one+qq(8)*fftem)
anu(7)=sqrt(eps(7)-(sin(phi))**2)
qqtem=(bh(8)/bh(7))*(anu(7)/anu(8))*ff(8)
qq(7)=(qqtem+one)/(qqtem-one)
fftem1=cplx(0.0d0, -wnum*two*al(7)*anu(7))
fftem=exp(fftem1)
ff(7)=(one+qq(7)*fftem)/(-one+qq(7)*fftem)
anu(6)=sqrt(eps(6)-(sin(phi))**2)
qqtem=(bh(7)/bh(6))*(anu(6)/anu(7))*ff(7)
qq(6)=(qqtem+one)/(qqtem-one)
fftem1=cplx(0.0d0, -wnum*two*al(6)*anu(6))
fftem=exp(fftem1)
ff(6)=(one+qq(6)*fftem)/(-one+qq(6)*fftem)
anu(5)=sqrt(eps(5)-(sin(phi))**2)
qqtem=(bh(6)/bh(5))*(anu(5)/anu(6))*ff(6)
qq(5)=(qqtem+one)/(qqtem-one)
fftem1=cplx(0.0d0, -wnum*two*al(5)*anu(5))
fftem=exp(fftem1)
ff(5)=(one+qq(5)*fftem)/(-one+qq(5)*fftem)
anu(4)=sqrt(eps(4)-(sin(phi))**2)
qqtem=(bh(5)/bh(4))*(anu(4)/anu(5))*ff(5)
qq(4)=(qqtem+one)/(qqtem-one)
fftem1=cplx(0.0d0, -wnum*two*al(4)*anu(4))
fftem=exp(fftem1)
ff(4)=(one+qq(4)*fftem)/(-one+qq(4)*fftem)
anu(3)=sqrt(eps(3)-(sin(phi))**2)
qqtem=(bh(4)/bh(3))*(anu(3)/anu(4))*ff(4)
qq(3)=(qqtem+one)/(qqtem-one)
fftem1=cplx(0.0d0, -wnum*two*al(3)*anu(3))
fftem=exp(fftem1)
ff(3)=(one+qq(3)*fftem)/(-one+qq(3)*fftem)
anu(2)=sqrt(eps(2)-(sin(phi))**2)
qqtem=(bh(3)/bh(2))*(anu(2)/anu(3))*ff(3)
qq(2)=(qqtem+one)/(qqtem-one)

```

```
fftem1=cplx(0.0d0,-wnum*two*al(2)*anu(2))
fftem=exp(fftem1)
ff(2)=(one+qq(2)*fftem)/(-one+qq(2)*fftem)
qqtem=(cos(phi)/anu(2))*ff(2)
qq(1)=(qqtem+bh(1)/bh(2))/(qqtem-bh(1)/bh(2))
fftem1=cplx(0.0d0,-wnum*two*al(1)*cos(phi))
fftem=exp(fftem1)
ff(1)=(one+qq(1)*fftem)/(-one+qq(1)*fftem)
ref=(ff(1)+bhl/bh(1))/(ff(1)-bhl/bh(1))
refr=real(ref)
refi=aimag(ref)
refabs=sqrt(refr**2+refi**2)
refdb=20.0d0*log10(refabs)
refarg=atan(refi/refr)
write (1,20) fr,refabs,refdb,refarg
20 format(1x,f5.2,1x,f8.5,1x,f6.2,
$1x,f8.3)
10 continue
stop
end
```